Coordination of Recombination with Meiotic Progression in the *Caenorhabditis elegans* Germline by KIN-18, a TAO Kinase That Regulates the Timing of MPK-1 Signaling

Yizhi Yin, Sean Donlevy, and Sarit Smolikove[1]
Department of Biology, University of Iowa, Iowa City, Iowa 52242

ABSTRACT Meiosis is a tightly regulated process requiring coordination of diverse events. A conserved ERK/MAPK-signaling cascade plays an essential role in the regulation of meiotic progression. The Thousand And One kinase (TAO) kinase is a MAPK kinase kinase, the meiotic role of which is unknown. We have analyzed the meiotic functions of KIN-18, the homolog of mammalian TAO kinases, in *Caenorhabditis elegans*. We found that KIN-18 is essential for normal meiotic progression; mutants exhibit accelerated meiotic recombination as detected both by analysis of recombination intermediates and by crossover outcome. In addition, ectopic germ-cell differentiation and enhanced levels of apoptosis were observed in *kin-18* mutants. These defects correlate with ectopic activation of MPK-1 that includes premature, missing, and reoccurring MPK-1 activation. Late progression defects in *kin-18* mutants are suppressed by inhibiting an upstream activator of MPK-1 signaling, KSR-2. However, the acceleration of recombination events observed in *kin-18* mutants is largely MPK-1-independent. Our data suggest that KIN-18 coordinates meiotic progression by modulating the timing of MPK-1 activation and the progression of recombination events. The regulation of the timing of MPK-1 activation ensures the proper timing of apoptosis and is required for the formation of functional oocytes. Meiosis is a conserved process; thus, revealing that KIN-18 is a novel regulator of meiotic progression in *C. elegans* would help to elucidate TAO kinase's role in germline development in higher eukaryotes.

KEYWORDS KIN-18; MPK-1; TAO; meiosis; recombination; genetics of sex

THE germline contains a multitude of cells that proliferate to form a population that will undergo two meiotic divisions, giving rise to gametes. In meiosis, one round of DNA replication is followed by two cell divisions reducing the ploidy of the germ cell by half. A large fraction of the cells encompassing the germline are found in meiotic prophase I. Many of the key evolutionarily conserved events that take place in this specialized prophase are aimed at preparing chromosomes for their segregation in meiosis I. One such essential and conserved event is the formation of crossovers between homologous chromosomes. During the initial stages of meiotic prophase I (leptotene/zygotene), a protein structure named the synaptonemal complex (SC) starts to assemble between homologs (MacQueen *et al.* 2002; Schild-Prufert *et al.* 2011). Concurrently, meiotic DNA double-strand breaks (DSBs) are introduced to initiate meiotic recombination (Keeney *et al.* 1997; Dernburg *et al.* 1998). As meiosis progresses, germ cells enter pachytene where the SC is fully formed and meiotic DSBs are processed and repaired. In the presence of a fully formed SC, meiotic DSBs are repaired, giving rise to crossovers by late pachytene. In most multicellular organisms, apoptosis is activated in late pachytene and reduces the number of germ cells in the developing germline (Gumienny *et al.* 1999). Apoptosis serves as a quality control mechanism and assists in the growth of the surviving oocytes; dying cells serve as "nurse cells" (Andux and Ellis 2008). The timely occurrence of each stage of meiosis is required for the formation of functional euploid gametes. Therefore, mechanisms assuring the timely progression of meiotic events must exist in *Caenorhabditis elegans* as well as in other organisms.

Mitogen-activated protein kinase (MAPK) pathways regulate intracellular signaling in response to various extracellular

doi: 10.1534/genetics.115.177295
Manuscript received April 12, 2015; accepted for publication October 23, 2015; published Early Online October 28, 2015.
Supporting information is available online at www.genetics.org/lookup/suppl/doi:10.1534/genetics.115.177295/-/DC1.
[1]Corresponding author: Department of Biology, 129 E. Jefferson, University of Iowa, Iowa City, IA 52242. E-mail: sarit-smolikove@uiowa.edu

stimuli (Widmann *et al.* 1999; Pearson *et al.* 2001). MAPK signaling cascades consist of terminal kinase MAPK and two upstream kinases, MAP2K and MAP3K. Three well-characterized subfamilies of MAPK are activated by specific upstream kinases in response to different stimuli: ERK, JNK, and p38 (Widmann *et al.* 1999; Pearson *et al.* 2001). The conserved ERK/MAPK-signaling cascade regulates meiotic progression in both vertebrate and invertebrate systems (Church *et al.* 1995; Fan and Sun 2004; Lee *et al.* 2007). In the *C. elegans* germline, the ERK ortholog MPK-1 is activated by upstream members LET-60/Ras, LIN-45/Raf (MAP3K), and MEK-2/Mek (MAP2K) along with the scaffold protein KSR-2 (Church *et al.* 1995; Hsu *et al.* 2002; Ohmachi *et al.* 2002). MPK-1 activation is temporally regulated: it is activated in pachytene, deactivated in diplotene, and then reactivated in proximal diakinesis oocytes (Lee *et al.* 2007). MPK-1 activation at pachytene is influenced by nutrient state and is mediated by the DAF-2 pathway (Lopez *et al.* 2013). Loss-of-function (*lf*) alleles of MPK-1 pathway members arrest prior to diplotene, indicating that MPK-1 activation is essential for normal meiotic progression (Church *et al.* 1995; Gumienny *et al.* 1999). The arrested nuclei cluster and eventually degenerate (Church *et al.* 1995; Hsu *et al.* 2002; Ohmachi *et al.* 2002). As wild-type nuclei progress through diplotene, MPK-1 is deactivated by LIP-1, a MAPK phosphatase, and oocytes remain arrested in prophase I at diakinesis (Hajnal and Berset 2002; Rutkowski *et al.* 2011). Then a signal from sperm, mediated by the major sperm protein, triggers the activation of MPK-1 in the proximal diakinesis oocyte. This activation leads to exit from meiotic prophase I and to the initiation of ovulation and the meiotic divisions (Miller *et al.* 2001; Kosinski *et al.* 2005).

Thousand And One (TAO) kinases were originally identified as mammalian homologs of Ste20 protein kinase in *Saccharomyces cerevisiae* (Hutchison *et al.* 1998; Chen *et al.* 1999). In mammalian tissue culture, TAO kinases function as a MAP3K that can activate p38 (MAPK) during stress response to trigger a cell cycle checkpoint (Hutchison *et al.* 1998; Chen *et al.* 1999, 2003; Chen and Cobb 2001; Yustein *et al.* 2003; Raman *et al.* 2007). TAOs were also shown to modulate actin cytoskeletal organization via JNK (MAPK) activation (Moore *et al.* 2000). Mammalian TAO1 and TAO2 expression is enriched in the testis, suggesting potential roles in the germline (Hutchison *et al.* 1998; Yustein *et al.* 2003). However, while the role of TAOs has been studied extensively in tissue culture and in somatic tissues, little is known about the function of TAO kinases in the germline.

Here we use *C. elegans* as a model system to investigate the germline function of TAO kinase. KIN-18 is the sole ortholog of TAO kinases in *C. elegans* and shares high sequence similarity in the kinase domain with both mammalian TAO1 and TAO2 (Hutchison *et al.* 1998). Previous publications have shown that KIN-18 is involved in the pharynx response during feeding and cell polarity in early embryonic development (Berman *et al.* 2001b; Spiga *et al.* 2013). Here we report the first direct evidence for the function of TAO kinase in meiosis by analyzing KIN-18's role in the germline of *C. elegans*. Loss of KIN-18 leads to accelerated prophase I progression, aberrant oocyte development, and ectopic apoptosis. Our data indicate that the late-prophase defects result from the incorrect activation via phosphorylation of a specific isoform of MPK-1.

Materials and Methods

Strains

All strains were cultured under standard conditions at 20° (Brenner 1974). N2 worms were utilized as the wild-type background. The following mutations and chromosome rearrangements were used (Ohmachi *et al.* 2002; Zou *et al.* 2009; Yokoo *et al.* 2012; Spiga *et al.* 2013): LGI—*hT2[bli-4(e937) qIs48]*, *ksr-2(dx27)*, *glp-4(bn2)* and LGIII—*kin-18(ok395)*. The following transgenic lines were used: *meIs8(GFP::COSA-1)* and *smIs34 [ced-1p::ced-1::GFP+rol-6(su1006)]*. All strains were outcrossed six times.

Analyses of the ok395 allele transcripts by RT-PCR

To determine if the deletion in *ok395* mutants is in frame or out of frame, we conducted RT-PCR analyses. This was done using the Superscript III OneStep RT PCR kit (12574-026, Life Technologies) and primers ATGGCGCCTGCCGTCTTACAAA and GAAGATTACTGAGTTGTTGCCTG for *kin-18* transcript isoform a (T17E91.a); and ATGGCGCCTGCCGTCTTACAAA and TTAGCCGTGGTTTTCATTTCC for *kin-18* isoform b (T17E91.b). KIN-18 gene has two isoforms reported (http://www.wormbase.org). Isoform a is predicted to have 11 exons with 2969 bp while isoform b is composed of the first 4 exons, most of exon 5 (last 24 bp are absent), and a specific, short exon 6 (17 bp) with a total length of 1062 bp. Our RT-PCR sequence reveals that the *ok395* allele is an in-frame deletion removing a protein-coding region spanning exon 2 through exon 7 of the isoform a transcript (Supporting Information, Figure S1; File S1). We did not observe any transcripts for isoform b in *kin-18(ok395)*.

Fecundity assay

To determine the fecundity of the *kin-18* mutants, single L4 worms were placed on seeded NGM plates and allowed to lay eggs for a 15-hr period. These worms were then moved to a fresh NGM plate and again allowed to lay eggs. This was repeated for 3 days. Following worm transfer, eggs were counted for each genotype examined. We counted the L1 and adults on each plate on the days following.

Apoptosis analysis

Germ-cell corpses were scored in adult hermaphrodites 18–20 hr post-L4 (Kelly *et al.* 2000; Zou *et al.* 2009). Statistical comparisons between genotypes were performed using the two-tailed Mann–Whitney test (95% C.I.).

Western blot

L4 homozygote larvae were picked and grown for 18–20 hr before flash-freezing in liquid nitrogen. The mouse α-MAPK-YT

(Sigma, 1:2000) was used as a primary antibody for dpMPK-1 (Lee *et al.* 2007). The rabbit α-ERK1/2 (SC94, 1:10,000) was used as primary antibody for total MPK-1 (Lee *et al.* 2007). Mouse α-tubulin (1:5000; *Developmental Studies Hybridoma Bank*) was used as a loading control. Secondary antibodies used were α-mouse and α-rabbit antibodies conjugated to horseradish peroxidase (1:10,000 and 1:20,000 respectively). PBST-5% milk was used for blocking and PBST-1% BSA was used for primary incubation. Quantification was done on FIJI following National Institutes of Health guidelines.

Immunostaining and microscopy

All immunostaining and whole-worm preparation was performed on synchronized 18- to 20-hr post-L4 adults. Whole-worm preparation was performed by standard carnoy fixation. Immunostaining for RAD-51, SYP-1 (double staining), and dpMPK-1 were performed as described (Brockway *et al.* 2014). Primary antibodies were used at the following dilutions: rabbit α-RAD-51 (1:10,000) (ModEncod), mouse α-MAPK-YT (1:400), goat α-SYP-1 (1:500), rabbit α- PH3 (1:5000), rabbit α-HTP-3 (1:500), and rabbit α-HIM-3 (1:500). The secondary antibodies used were Alexa Fluor 488 α-Rabbit (1:500), Alexa Fluor 488 α-mouse (1:500), and DyLight 594 α-goat (1:500). Membrane was stained with agglutinin conjugated to fluorescein (Vector FL-1071), and cell width on the longer axis of each oocyte at the 60- × 60-μm most-proximal region was measured using softWoRx software (Applied Precision). GFP::COSA-1 foci microscopic analysis was performed as previously described (Yin and Smolikove 2013). The images were acquired using the DeltaVision wide-field fluorescence microscope system (Applied Precision) with Olympus 100X/1.40 lenses for SYP-1, RAD-51, and COSA-1 and a 60X/1.40 lens for dpMPK-1. Optical sections were collected at 0.20-μm increments with a coolSNAP$_{HQ}$ camera (Photometrics) and softWoRx software (Applied Precision) and deconvolved using softWoRx 5.0.0 software for SYP-1, RAD-51, and COSA-1.

For dpMPK-1 staining, all mutants were dissected with wild-type worms on the same slide. Mutants and wild-type germlines were differentiated by DAPI morphology. Only slides with successful (>90%) dpMPK-1 staining wild-type worms were scored for dpMPK-1 staining pattern. Single-panel images were taken for dpMPK-1 staining. Images were processed as in Lopez *et al.* (2013).

RAD-51 and COSA-1 foci quantification

Germlines were divided by 42-μm^2 zones, and images were taken from the premeiotic tip at the most-proximal end. The meiotic stages of nuclei were decided based on SYP-1 morphology along with their position in the germline. Transition zone was counted starting with the row of nuclei containing ≥60% nuclei exhibiting foci or short noncontinuous stretches of SYP-1 morphology with a crescent-shaped chromosome. Early pachytene was counted, starting with the row of nuclei containing ≥60% nuclei exhibiting continuous but not-dispersed SYP-1 threads. Middle pachytene was counted starting with the row of nuclei containing ≥60% nuclei exhibiting continuous and dispersed SYP-1 threads. Diplotene was counted starting with the row of nuclei containing nuclei with discontinuous condensed SYP-1 morphology. Diakinesis was identified as nuclei with condensed DAPI bodies with stretches of SYP-1 threads. For number of gonads and nuclei scored per type, see Table S1.

Data availability

Strains are available upon request.

Results

KIN-18 is required for normal meiotic progression in C. elegans

To determine if KIN-18 functions in meiosis, we analyzed the deletion mutant *kin-18(ok395)* (Spiga *et al.* 2013). The *ok395* allele produces a truncated messenger RNA that results in an in-frame 596-amino-acid (aa) deletion at the N terminus of both isoforms (Figure S1). This leads to 60% deletion of aa sequence of isoform a and 85% of isoform b and complete deletion of the predicted kinase domain as well as the predicted target binding domain (Berman *et al.* 2001b). Thus, the remaining truncated protein in *ok395* is likely to be inactive.

kin-18 mutants are completely sterile with a brood size of 0 ± 0 (mean ± SD, wild-type brood size 286 ± 22, Mann–Whitney test, two-tailed, $P < 0.01$, $n = 10, 5$). The sterility observed in *kin-18* mutants cannot be suppressed by mating to wild-type males (0 ± 0, $n = 9$). This indicates that KIN-18 is required for the production of embryos via its role in oogenesis.

To identify the causes for this sterility, *kin-18* and wild-type hermaphrodites were fixed and stained with DAPI to visualize chromosomes. The *C. elegans* germline consists of two syncytial U-shaped gonads with nuclei arranged in a distal-to-proximal polarity with the mitotic tip (MT) at the distal end while mature oocytes and the spermatheca are found at the proximal end. Nuclei in the MT undergo proliferation to generate germline nuclei that enter meiosis (leptotene/zygotene) in a region termed the transition zone (TZ); this is followed by nuclei entering and progressing through pachytene (PT). The bend region of the U-shaped gonad contains nuclei transitioning from pachytene to diplotene. Diplotene nuclei will mature into diakinesis oocytes, as they become cellularized. Wild-type gonads show a highly ordered progression of nuclei in meiotic prophase I: pachytene nuclei are found before the bend region, and a single row of oocytes is observed following the bend region (Figure 1, A, C, and D). Based on our whole-worm analysis, *kin-18* mutants have shorter gonads with mostly normal progression through middle pachytene (Figure 1B). However, the nuclei found subsequent to pachytene exhibit an abnormal meiotic progression with a mixture of diakinesis-like and pachytene-like nuclei before and after the bend region (Figure 1, B, E, and F). We define this mixed positioning (pre- and post-bend) of

diakinesis nuclei as ectopic oocyte differentiation. Later analysis (see below) identified additional characteristics of ectopic oocyte differentiation and strengthened the argument that diakinesis oocytes defined by DAPI are indeed diakinesis oocytes.

In addition to the changes in meiotic progression, we also observed reduction in total nuclei numbers in *kin-18* mutants. Wild-type gonads had an average of 687 ± 34 nuclei (mean ± SE) per gonad, and *kin-18* worms had a significant reduction in the overall number of nuclei in the germline to 223 ± 7 (Mann–Whitney test, two-tailed, $P < 0.01$, Figure 1I). Division of nuclei at the mitotic tip is required for germline proliferation and determines the number of germline nuclei prior to the bend region (where apoptosis clears out nuclei). The overall reduction in the number of germline nuclei in *kin-18* mutants can be attributed to changes in the cell cycle of the mitotically proliferating nuclei. We performed staining to the phosphorylated form of histone H3 (PH3), a marker for metaphase in wild-type and *kin-18* worms. The ratio of PH3-positive nuclei to the total number of mitotic nuclei determines the mitotic index (Crittenden *et al.* 2006). We observed an increase in the mitotic index (PH3-positive cells/mitotic tip nuclei) in *kin-18* mutants (mean ± SE: 3.73 ± 0.27 in wild type; mean ± SE: 7.01 ± 0.7 in *kin-18* mutants; Figure S2D). Increased mitotic index can be a result of increased numbers of nuclei entering metaphase or increased numbers of nuclei lingering on in metaphase. Since the total number of nuclei in the *kin-18* mutants was reduced, mitotic proliferation is likely reduced and not increased in *kin-18* mutants, indicating that the increase in the mitotic index reflects a metaphase arrest or prolonged metaphase in some of the nuclei in the mitotic zone.

A standard approach to the analysis of the *C. elegans* germline involves dividing the germline into equal-size zones (see *Materials and Methods*), followed by quantitative analysis of meiotic events in each of these zones. Zones 1 and 2 are composed mainly of mitotic nuclei (premeiotic tip) undergoing proliferation to generate the nuclei population that enters meiosis in the next region, termed the "transition zone" (mostly zone 3). The nuclei in the transition zone are in the leptotene/zygotene stages and acquire a typical clustered (polarized) chromosomal organization and discontinuous, partially assembled SC. At pachytene (zones 4–7), chromosomes disperse from polarized organization, and the SC becomes linear and fully formed. Toward the end of pachytene (zones 6 and 7), nuclei either undergo physiological apoptosis or progress from diplotene to diakinesis, differentiating into oocytes (Gumienny *et al.* 1999). The SC undergoes stepwise disassembly starting in late pachytene (zone 7) through diplotene (zone 8) and diakinesis (zone 9–13). Bivalents are then connected only by crossovers and sister-chromatid cohesion (Schvarzstein *et al.* 2010). Late diakinesis nuclei cellularize to form oocytes and remain arrested with six bivalents until ovulation is triggered by sperm (Miller *et al.* 2001; Kosinski *et al.* 2005).

The germline of *kin-18* mutants was smaller with reduced numbers of nuclei per zone compared to wild type (Figure 1I and Table S1). Without having a marker for meiotic progression that can differentiate all of the meiotic stages it is difficult to assess which nuclei are at any particular meiotic stage in *kin-18* mutants. Meiotic stages are defined by chromosome structure and SC morphology (Zickler and Kleckner 1999). Studies in mice frequently use the morphology of the SC and chromosome morphology (by DAPI staining), based on examination of immunofluorescence preparation, as an indication of the meiotic stage of germline nuclei (Cole *et al.* 2012; Kauppi *et al.* 2013; Qiao *et al.* 2014). We adopted this metric to investigate meiotic progression in *kin-18* mutants.

First, we tested whether SC morphology was altered in *kin-18* mutants by using antibodies against HTP-3/HIM-3, SC axial components, and SYP-1, a central region protein of the SC (MacQueen *et al.* 2002). Using this method, *kin-18* mutants showed no defects in SC assembly. This includes axis assembly prior to central region assembly and the gradual localization of SYP-1 onto chromosomes at meiotic entry followed by linear localization between pairs of chromosomes (Figure 2 and Figure S3). Although the position of meiotic nuclei in the gonad was altered (as discussed above), we did not observe any defects in chromosome morphology; chromosomes clustered at meiotic entry and dispersed as aligned tracks in later stages, and then nuclei with condensed and compact bivalents were observed. Therefore, the pattern of SC assembly in combination with chromosome organization could be used as an indication for the meiotic stage of each nucleus (*Materials and Methods* and Figure 2), similarly to the method used to determine the stages of meiosis in mice (Cole *et al.* 2012; Kauppi *et al.* 2013; Qiao *et al.* 2014). This method allowed us to determine the position in the gonad where nuclei move from the transition zone to early pachytene or from early pachytene to mid-pachytene.

Consistent with the whole-worm analysis (Figure 1, B, E, and F), *kin-18* gonads displayed a mixture of diplotene/diakinesis and pachytene nuclei in the proximal region (Figure 2). We normalized the number of nuclei at each stage (based on SYP-1 and DAPI staining) to the total number of nuclei in the germline (Figure 1J). This normalization allowed us to examine whether any particular meiotic stage was over- or underrepresented in *kin-18* mutants as compared to wild type. We observed a small, but statistically significant, decrease in the percentage of nuclei in early stages of meiosis (TZ, two-tailed Fisher's exact test, $P < 0.001$), no change in early prophase (EP, two-tailed Fisher's exact test, $P > 0.05$), and an increase in the percentage of nuclei in late prophase [middle and late pachytene (M/LP) and diplotene and diakinesis (DP DK), two-tailed Fisher's exact test, $P < 0.001$; Figure 1J, Table S1, and Table S2]. These shifts may indicate that meiotic progression is accelerated in *kin-18* mutants accompanied by irregular pachytene exit (as supported by additional findings; see below).

The proximal gonad of *kin-18* mutants contained nuclei with diakinesis chromosome morphology. However, unlike the late diakinesis bivalents of wild type, which are spaced from each other, these bivalents were positioned in proximity to each other. This was likely due to the overall smaller

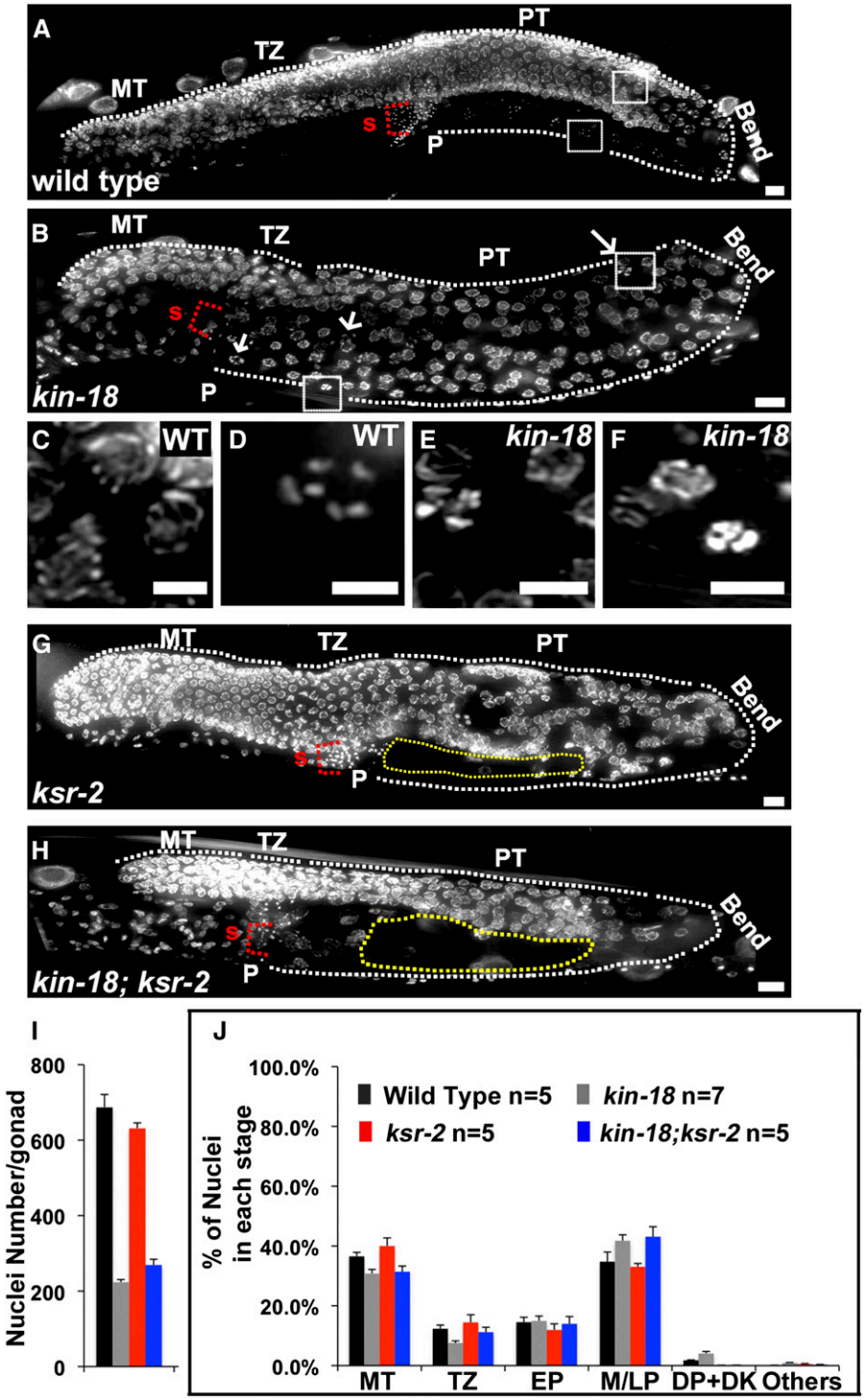

Figure 1 Germline morphology defects in *kin-18* mutants. DAPI-stained whole-worm preparation for young adults of (A) wild type, (B) *kin-18*, (G) *ksr-2*, and (H) *kin-18*; *ksr-2* double mutants. White dotted line depicts the edge of the germline. P, proximal end; S, sperm. Yellow dotted line in G and H depicts area devoid of nuclei. Bar, 10 mm. Panel A, B G, and H shows a projection of a three-dimensional stack of half the gonad. Arrows indicate an example for diakinetic-like nuclei in *kin-18* mutants. (C) Zoom in image of representative pachytene nuclei prior to the bend region in wild type (zoom-in near the pre-bend region boxed in A). (D) Zoom-in image of representative diakinesis oocytes in post-bend region in wild type (zoom-in near the post-bend region boxed in A). (E) Zoom-in image nuclei prior to bend in *kin-18* mutants (zoom-in near the pre-bend region boxed in B). (F) Zoom-in image of nuclei in the post-bend region of *kin-18* mutants (zoom-in of region near the post-bend region boxed in B). Bar, 5 mm. Each panel shows a projection of a three-dimensional stack of the whole nuclei. Quantification of nuclei number (I) and percentage of nuclei at different meiotic stages (J) in different genotypes. MT, mitotic tip; TZ, transition zone; EP, early pachytene; M/LP, middle and late pachytene; DP/DK, diplotene and diakinesis; Others, apoptotic nuclei or nuclei with condensed or loose DAPI bodies that do not resemble nuclei in any meiotic stage.

volume of oocytes of *kin-18* mutants (indicated by measurement of cell width) (Figure S4). Further analysis indicated that these nuclei were indeed diakinesis nuclei because they (1) show localization of PH3, typical for late diakinesis nuclei (Figure S2, E and F), and (2) lose localization of GLD-1 only in proximal nuclei with diakinesis chromosome morphology (Figure S5), indicating pachytene exit in these nuclei. Despite the normal assembly of the SC in *kin-18* mutants, the SC disassembled aberrantly in *kin-18* mutants; in wild-type, SYP-1 and PH3 localization is mostly restricted to the mid-bivalent region (the short arm of the bivalent) (Nabeshima *et al.* 2005), while, in *kin-18* mutants, SYP-1 and PH3 stained both bivalent arms more frequently (both arms: wild type, 9%; *kin-18*, 81%; Table S3, Figure 2, and Figure S2, E and F). This indicates that, although oogenesis is taking place in *kin-18* mutants, it is aberrant (small oocytes with defects in SC disassembly).

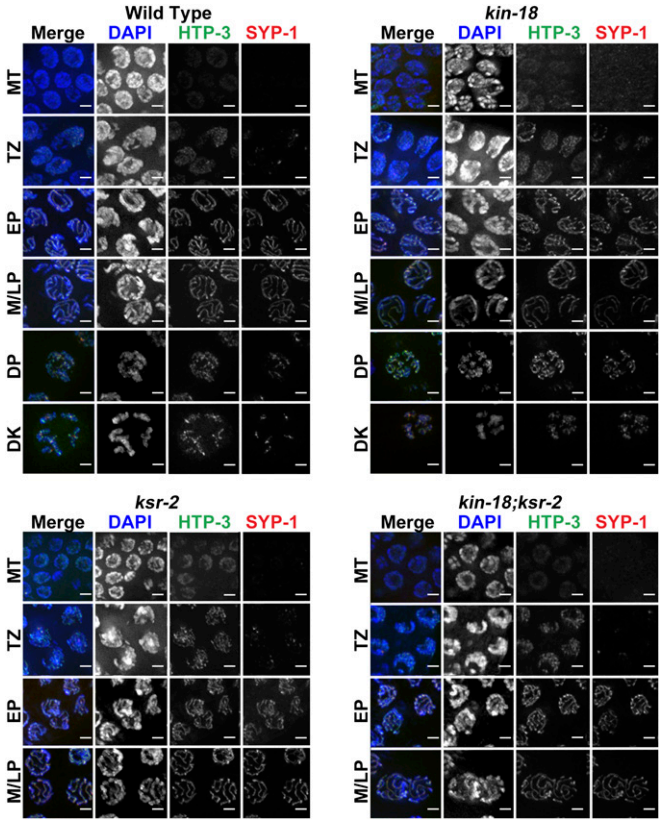

Figure 2 SYP-1 and HTP-3 localization in wild-type and *kin-18* worms. Images of nuclei at different stages (as indicated): wild-type, *kin-18*, *ksr-2*, and *kin-18;ksr-2* double mutants. MT, mitotic tip; TZ, transition zone; EP, early pachytene; M/LP, middle/late pachytene; DP, diplotene; DK, diakinesis. Blue, DAPI; red, SYP-1; green, HTP-3. Bar 2 μm.

Early meiotic prophase I events are accelerated in kin-18 mutants

To test our hypothesis that progression through early prophase I was accelerated in *kin-18* mutants, we analyzed the progression of a key meiotic event in early prophase I: homologous recombination. Meiotic recombination initiates in early prophase I by DSB formation and resection to ultimately form crossovers (Dernburg *et al.* 1998). To analyze meiotic recombination progression, we used RAD-51 and COSA-1 proteins as markers for DSB resection and crossover formation, respectively. RAD-51 is a single-strand (ssDNA)-binding protein that loads on resected (ssDNA) DSBs in early prophase (Alpi *et al.* 2003; Martin *et al.* 2005). RAD-51 is required for strand invasion that is the prerequisite to crossover formation (Martin *et al.* 2005). COSA-1 is a protein required for crossover formation that localizes to the one crossover found in each bivalent of *C. elegans* and therefore is a marker for late recombination events, marking crossovers as they are being processed in wild-type worms (Yokoo *et al.* 2012). RAD-51 and COSA-1 localization was analyzed using similar methods (divisions into zone and meiotic stages) as were used for SYP-1 localization (see *Material and Methods*).

In wild-type nuclei, RAD-51 loads onto chromosomes starting in early pachytene, and the number of foci peaks in middle pachytene (Figure 3, A and B; Figure S6; Figure S7). In *kin-18* worms, the loading of RAD-51 peaks earlier (in early pachytene) with higher RAD-51 foci levels compared to wild type (Mann–Whitney two-tailed test, $P < 0.001$; Figure 3, A and C; Figure S6; Figure S7; Table S4; Table S5; Table S6; Table S7). The high levels of RAD-51 foci decrease in middle pachytene in *kin-18* worms, resembling the number of foci per nucleus found in wild type at this stage (Figure 3A; Figure S6; Figure S7; Table S4; Table S5; Table S6). The earlier peak of RAD-51 foci (early pachytene *vs.* middle pachytene; Table S4 and Table S5) as well as an increase in the overall numbers of RAD-51 foci (Table S4 and Table S6) suggests that recombination timing is affected in *kin-18* mutants.

Consistent with an earlier peak of RAD-51 loading, a marker for late stages in crossover formation localized earlier in *kin-18* worms compared to wild type. Wild-type gonads exhibit six COSA-1 foci per nucleus at late pachytene (Figure 4, A, C, and E; Figure S8A, zone 6). In contrast, *kin-18* mutant gonads displayed COSA-1 foci already in early pachytene, when they were never observed in wild type (Figure 4, B, D, and F; Figure S8B, zones 2–3, two-tailed Mann–Whitney test, $P < 0.05$ of nuclei from EP). Compared to wild type, significant enrichment of nuclei with crossovers/COSA-1 was also found in the mid- to late pachytene stages of *kin-18* mutants (Figure 4, B, D, and F; Figure S8B, two-tailed Mann–Whitney test, $P < 0.001$ of nuclei from M/LP).

Absence of KIN-18 leads to ectopic and elevated apoptosis

In *C. elegans* about half the gonad's nuclei undergo physiological apoptosis (at the bend region), and the surviving nuclei differentiate into oocytes (Gumienny *et al.* 1999). We observed an ectopic oocyte differentiation in *kin-18* mutants around the same region in which apoptosis takes place in wild-type gonads (bend region, Figure 1). Therefore, we asked whether *kin-18* mutants also display ectopic apoptosis. We used both CED-1::GFP and acridine orange staining as markers for apoptosis (Kelly *et al.* 2000; Zou *et al.* 2009). In wild-type gonads, apoptosis occurred only in late pachytene nuclei, prior to the bend region (Figure 5, A′, C, and D). In *kin-18* mutants, apoptosis was not limited to around the bend region. Apoptosis was strikingly high after the bend region (toward the proximal end of the gonad), as indicated by both CED-1::GFP and acridine orange analysis (Figure 5, B′, C, and D). CED-1::GFP, but not acridine orange analysis, showed apoptotic nuclei also in the pre-bend region in *kin-18* gonads (Figure 5, B′ and C). This is likely due to CED-1::GFP marking different steps in apoptosis compared to acridine orange analysis and CED-1::GFP being a more sensitive marker (Gartner *et al.* 2008). However, both were consistent with high levels of apoptosis in the proximal gonadal region. This high level of ectopic apoptosis pattern correlates with the ectopic oocyte differentiation. Indeed, 2-day-old adults displayed reduction in nuclei numbers in the proximal gonad (Figure S9). This is consistent with nuclei

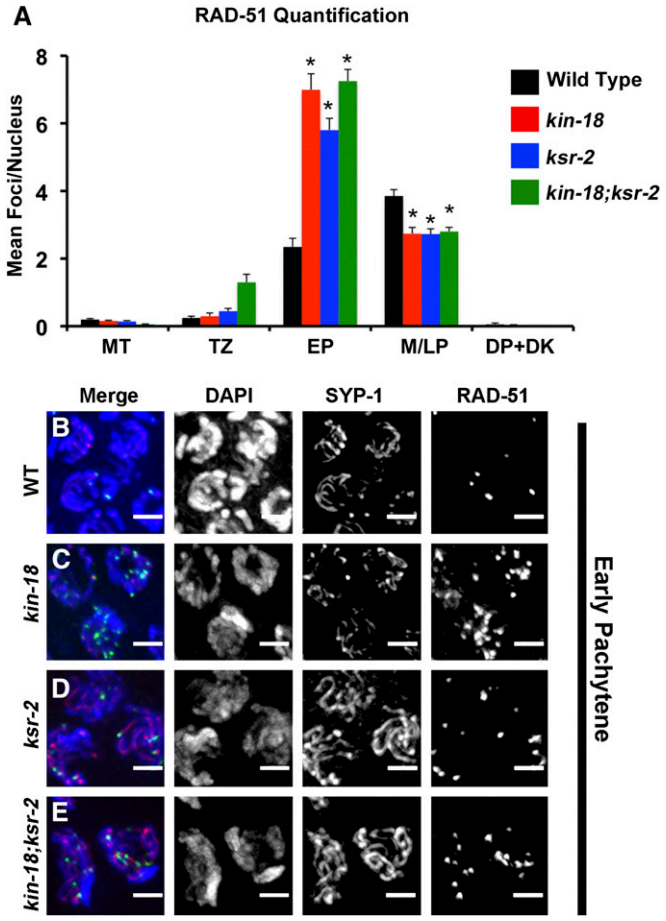

Figure 3 RAD-51 foci loading is accelerated in mutants with disturbed MPK-1 activation. (A) Quantification of the mean number of RAD-51 foci per nucleus at each meiotic stage. MT, mitotic tip; TZ, transition zone; EP, early pachytene; M/LP, middle and late pachytene. DP/DK, diplotene and diakinesis. *$P < 0.001$ (compared to wild-type Mann–Whitney two-tailed test, 95% C.I.). Number of nuclei counted and pairwise statistics are in Table S4, Table S5, and Table S6. (B–E) Representative images of representative nuclei in early pachytene in (B) wild type, (C) *kin-18*, (D) *ksr-2*, and (E) *kin-18;ksr-2*. Merge: Merge of DAPI, SYP-1, and RAD-51 channels. Images are projections of panels of one nuclei. Blue, DAPI; red, SYP-1; green, RAD-51. Bar 2 μm.

marked for apoptosis in day 1 being cleared by engulfment only by day 2. This also explains why no eggs were laid by the *kin-18* mutants. Together, these results support a role for KIN-18 in the regulation of the normal timing of apoptosis.

KIN-18 negatively regulates the activation of MPK-1a

The MPK-1/ERK-signaling pathway is the master regulator of germline development in *C. elegans* (Church *et al.* 1995; Lee *et al.* 2007). Since *kin-18* mutant gonads exhibit ectopic oocyte differentiation and apoptosis, we asked if MPK-1 activation is affected in the germline of *kin-18* worms.

MPK-1 consists of two isoforms: MPK-1a and MPK-1b. MPK-1a is an isoform activated mainly in somatic cells (Lee *et al.* 2007). One study suggests that MPK-1a is also expressed in the pachytene region of the germline, although in much lower levels than in the soma (Schouest *et al.* 2009). The MPK-1b isoform is present only in the germline and has been suggested to be specific to proximal oocytes (Schouest *et al.* 2009). Activation of MPK-1 in pachytene regulates pachytene exit whereas its activation in diakinesis is required for ovulation (Church *et al.* 1995; Lee *et al.* 2007). We performed Western blot analyses using an antibody (MAPK-YT) specific for both isoforms of the activated di-phosphorylated MPK-1 (dpMPK-1) (Lee *et al.* 2007). Protein extracts from wild-type whole worms show two bands, ~45 and ~55 kDa in size, corresponding to dpMPK-1a and dpMPK-1b, while *kin-18* mutants exhibit no dpMPK-1b but a threefold increase in dpMPK-1a (Figure 6, Mann–Whitney two tailed test, $P < 0.001$). To investigate if the amount of total MPK-1 is affected, we used an antibody that recognizes MPK-1 regardless of its phosphorylation state (Lee *et al.* 2007). *kin-18* mutants did not have a significant increase of the total amount of MPK-1a compared to wild type (Figure 6, Mann–Whitney two-tailed test, $P > 0.05$). The level of total MPK-1b was greatly reduced in *kin-18* mutants (Figure 6, Mann–Whitney two-tailed test, $P < 0.001$). These results indicate that activation of MPK-1a through phosphorylation is enhanced in the absence of KIN-18 and that this activation is not due to an effect on MPK-1a protein levels. In contrast to the normal levels of MPK-1a, MPK-1b protein levels were reduced in *kin-18* mutants, indicating that KIN-18 is required for MPK-1b expression in the germline.

KIN-18 is required for the normal timing of MPK-1a activation

To determine if KIN-18 regulates the timing of MPK-1 activation, we performed immunostaining with the same antibody used for Western blot analysis (MAPK-YT). Since the position of the nuclei in the germline roughly reflects their meiotic stage, altered positioning of dpMPK-1 staining indicates an altered timing of MPK-1 activation. Wild-type gonads display two regions of activation of MPK-1: the region of activation that spans middle-to-late pachytene and a region of activation in oocytes most proximal to sperm (Figure 7A). *kin-18* worms display an aberrant MPK-1 activation with 44% ($n = 43$) of the gonads showing no apparent activation, while 56% ($n = 43$) of gonads display activation at various positions (Figure 7B). Among gonads with aberrant MPK-1 activation, 33% ($n = 43$) exhibited one region of activation in various positions (Figure 7B). Among gonads with aberrant MPK-1 activation, 33% ($n = 43$) exhibited one region of activation (Figure 7B bottom) in various positions like the proximal end or early pachytene; the remaining 23% ($n = 43$) of gonads showed multiple regions of activation (Figure 7B top). Since Western blot analysis showed an absence of dpMPK-1b in *kin-18* mutants, we reasoned that the dpMPK-1 staining likely represents dpMPK-1a and that this isoform is ectopically activated. That is, MPK-1 is activated both at elevated levels and in aberrant positions (*i.e.*, in regions that normally lack MPK-1 activation in wild type).

Oocyte maturation and apoptosis in kin-18 mutants require canonical MPK-1/ERK signaling

To test our hypothesis that aberrant MPK-1 activation is responsible for the ectopic oocyte differentiation and apoptosis

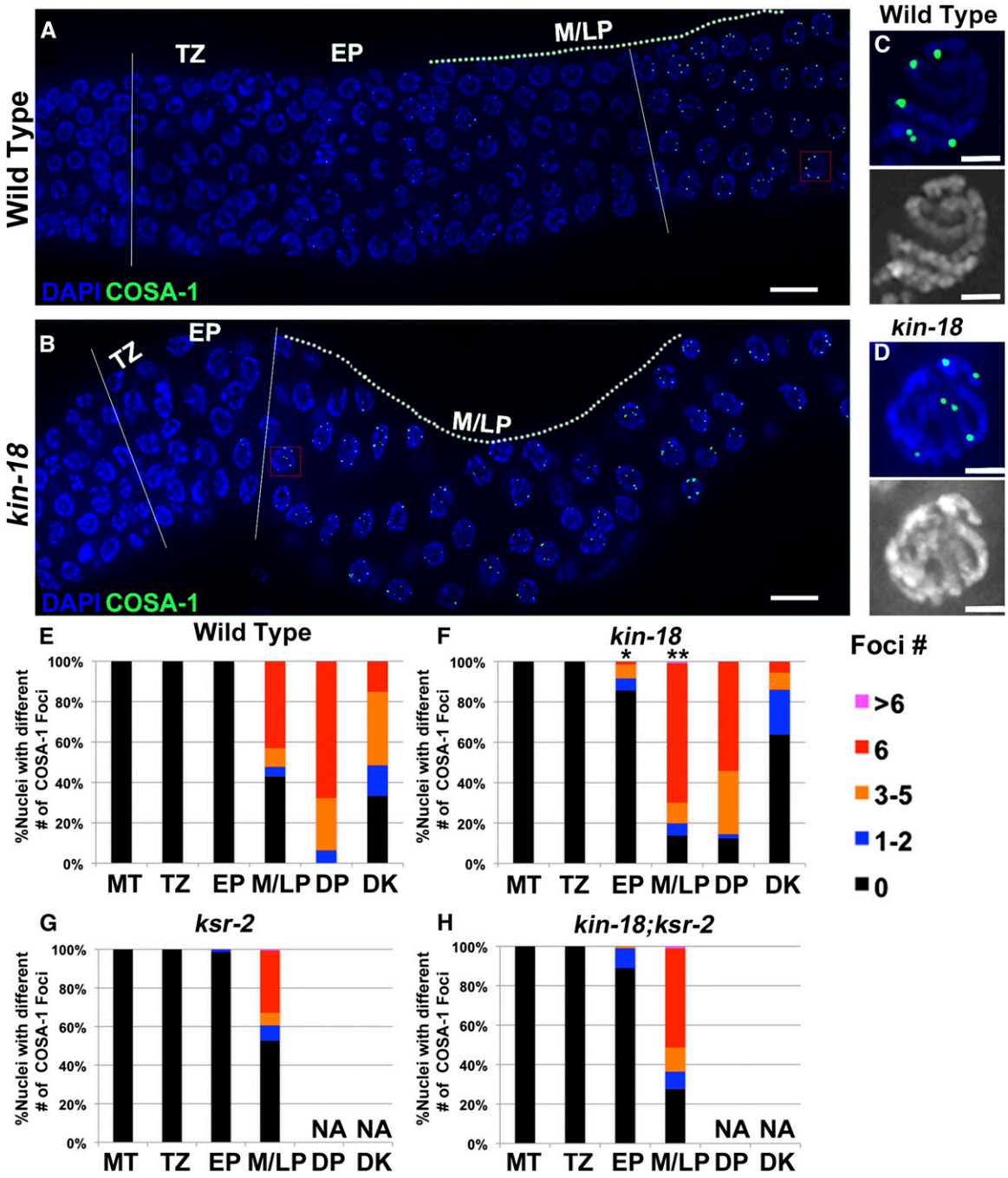

Figure 4 COSA-1 loading is accelerated in *kin-18* mutants. Representative images of gonad with COSA-1 foci from transition zone to late pachytene in (A) wild type and (B) *kin-18*. Dotted line depicts germline regions in middle and late pachytene. Two straight white lines depict the germline region between entry to meiosis to appearance of nuclei with six COSA-1 foci. Red square depicts the position of the zoom-in image of a representative nuclei with six COSA-1 foci in (C) wild type and (D) *kin-18*. Blue/white, DAPI; green, GFP:COSA-1. Bar: A and B, 10 μm; C and D, 2 μm. Percentage of nuclei with a different number of COSA-1 foci in (E) wild type, (F) *kin-18*, (G) *ksr-2*, and (H) *kin-18;ksr-2* double mutants. MT, mitotic tip, TZ, transition zone; EP, early pachytene; M/LP, middle and late pachytene; DP, diplotene; DK, diakinesis. Number of nuclei examined for wild type, *kin-18*, *ksr-2*, and *kin-18;ksr-2* are as follows: MT—320, 381, 430, 357; TZ—159, 116, 185, 130; EP—161, 133, 164, 97; M/LP—251, 562, 180, 116; DP—31, 48, 0, 0; DK—33, 36, 0, 0. Half of the nuclei from five wild-type and *ksr-2* gonads were counted. *kin-18* and *kin-18;ksr-2* did not have well-developed rachis, and thus three layers of nuclei from seven *kin-18* gonads were counted. $*P < 0.05$, $**P < 0.001$ (compared to wild type; Mann–Whitney two-tailed test, 95% C.I.).

in *kin-18* worms, we eliminated MPK-1 activation in *kin-18* mutants. KSR-2 is a scaffold protein required for MPK-1/ERK activation in *C. elegans*, via regulating MEK-2/MAP2K phosphorylation by LIN-45/MAP3K (Ohmachi *et al.* 2002). We combined the *ksr-2(dx27)* loss-of-function allele with the *kin-18* mutant allele to eliminate MPK-1 signaling in these *kin-18* mutants. A Western blot of *ksr-2* mutants is in agreement with the published absence of dpMPK-1b and a

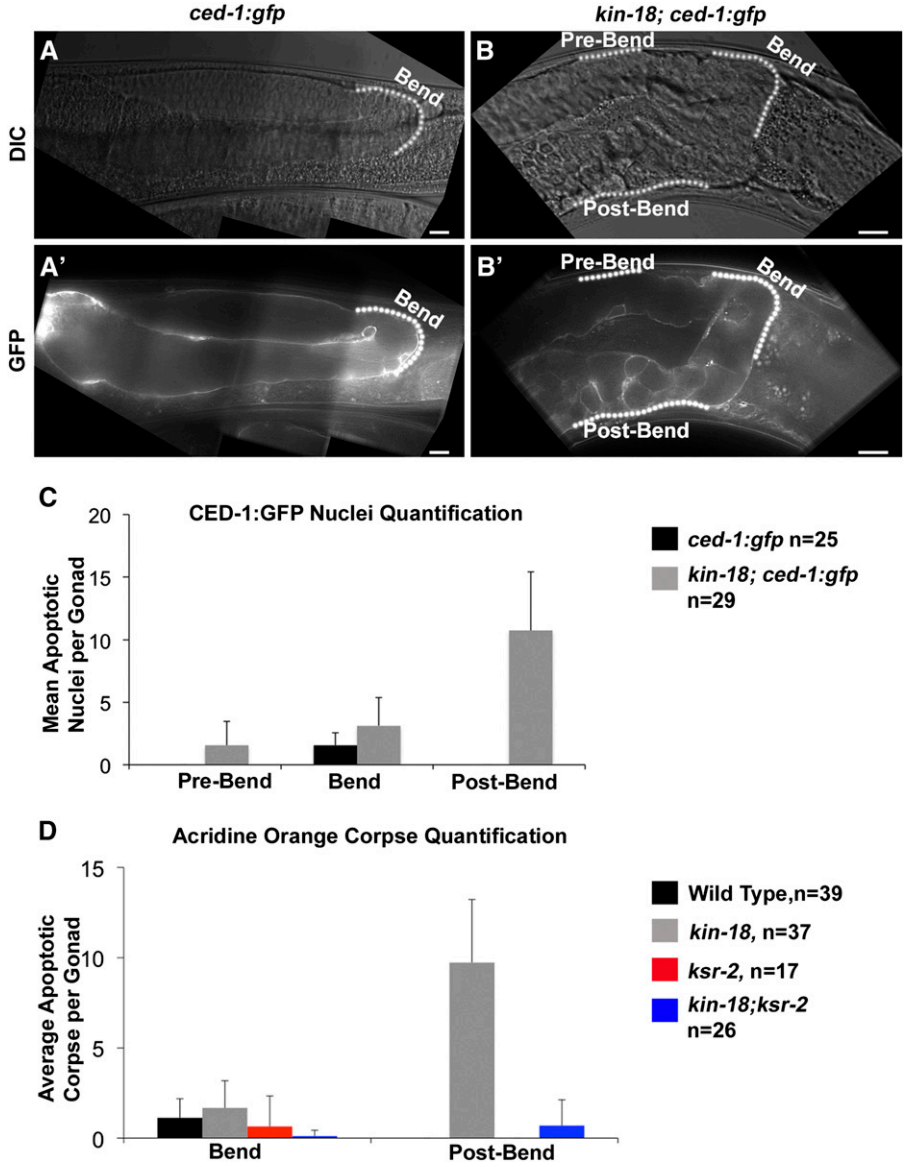

Figure 5 Ectopic apoptosis in *kin-18* mutants depends on MPK-1 activation. Images of gonad with apoptotic nuclei marked by CED-GFP of (A′) wild type and (B′) *kin-18*. A and B are images of DIC used to visualize the germline tissue of wild type and *kin-18*, respectively. Images are taken as a single panel. Bar, 10 μm. (C) Quantification of CED-1::GFP marked apoptotic nuclei per gonad based on its position relative to the bend region. (D) Quantification of acridine orange marked apoptotic nuclei per gonad based on the position (at bend region or post-bend region). $P < 0.01$ between wild type and *kin-18* for post bend in C and D (Mann–Whitney two-tailed test, 95% C.I.).

significant reduction in dpMPK-1a (Figure 6) (Ohmachi *et al.* 2002; Lee *et al.* 2007). Also, as published, the level of total MPK-1a and -b is not significantly affected in *ksr-2* mutants compared to wild type (Figure 6, Mann–Whitney two- tailed test, $P > 0.05$) (Lee *et al.* 2007). While we observe no germline immunostaining in *ksr-2*; *kin-18* worms, the presence of dpMPK-1a in whole-worm extracts suggests that *ksr-2* eliminates MPK-1 signaling in a germline-specific manner (Figure 7, C and D). These findings are in agreement with previous publications (*e.g.*, Ohmachi *et al.* 2002).

Our data suggest that *ksr-2* is epistatic to *kin-18*, regarding late events in meiotic prophase I. The proximal end of the gonad in *ksr-2;kin-18* double mutants was devoid of nuclei (no diplotene and diakinesis nuclei), a phenotype that is similar to *ksr-2* single mutants (Figure 1, G, H, and J; Table S1). Furthermore, our analysis also showed a significant reduction of apoptosis especially in the post-bend region (Figure 5D). These results suggest that the abnormal oocyte differentiation and apoptosis in *kin-18* mutants are due to aberrant activation of the canonical MPK-1/ERK-signaling pathway.

Normal dynamics of early recombination events depend on MPK-1 signaling

To investigate whether the acceleration and the increase in levels of RAD-51 foci in *kin-18* mutants depends on MPK-1 activation, we examined RAD-51 localization in *ksr-2* and *kin-18*; *ksr-2* double mutants. The numbers of RAD-51 foci in *ksr-2* mutants peak early—early pachytene, opposed to mid-pachytene (Figure 3, A and D; Figure S6; Figure S7)—and display an increased number of foci per nucleus (Figure 3A; Table S4; Table S5; Table S6). This phenotype is similar to that of *kin-18* single mutants. As found in *kin-18* mutants, *ksr-2* single mutants show an increase in the overall levels of RAD-51 foci (Mann–Whitney two-tailed test, $P < 0.001$; Table S4 and Table S6). The localization pattern of RAD-51 foci in the *kin-18*; *ksr-2* double mutants was similar to

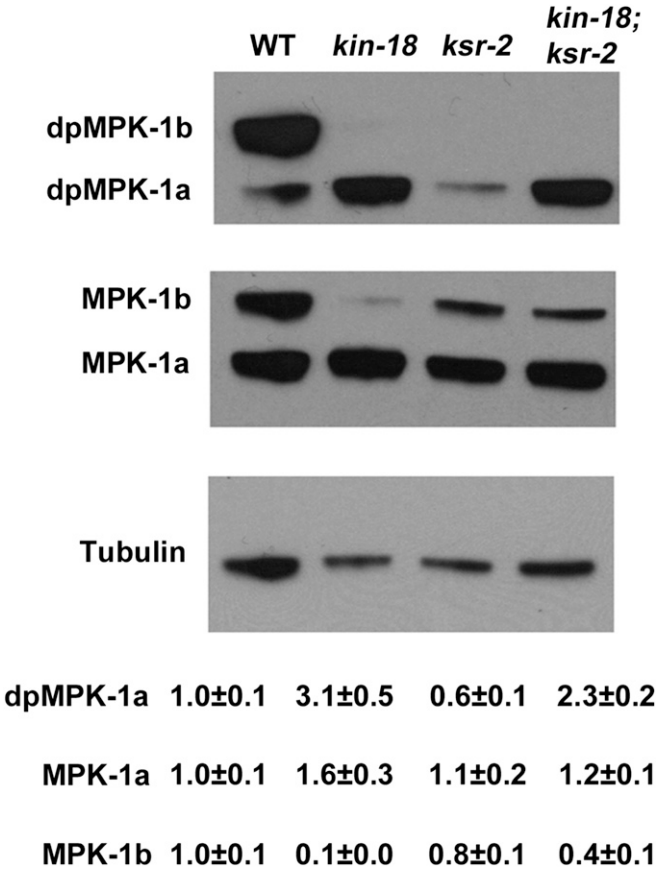

dpMPK-1a	1.0±0.1	3.1±0.5	0.6±0.1	2.3±0.2
MPK-1a	1.0±0.1	1.6±0.3	1.1±0.2	1.2±0.1
MPK-1b	1.0±0.1	0.1±0.0	0.8±0.1	0.4±0.1

Figure 6 Western blot analysis of dpMPK-1 and MPK-1 in mutants. Representative Western blots of dpMPK-1 (phosphorylated active MPK-1) and total MPK-1 (total MPK-1 regardless of phosphorylation) as well as loading control tubulin. Quantification is normalized to the amount of tubulin (n = 7 for all quantifications). All images and quantification for different antibodies were performed on the same blot stripped and reprobed.

that of *kin-18* mutants, consistent with both genes acting in the same pathway affecting RAD-51 localization (Figure 3, A and E; Figure S5; Figure S6; Table S4; Table S5; Table S6). In contrast to the effect of *kin-18* mutants on COSA-1 localization, *ksr-2* mutants did not exhibit premature formation of COSA-1 foci and did not completely suppress the phenotype of *kin-18* mutants (Figure 4; Figure S8; Figure S10; Table S8). Therefore, in respect to recombination, *kin-18* may be epistatic to *ksr-2*. This result indicates the effect of KIN-18 on early (recombination) *vs.* late (oocyte formation) meiotic events involving different pathways (see *Discussion*). All together these results suggest that early recombination events are altered when MPK-1 activation is abnormal, although some of the effects of KIN-18 on recombination may be MPK-1-independent.

Discussion

The data presented in this article indicate that KIN-18, the *C. elegans* ortholog of TAO kinases, is required for normal progression of meiotic events in the germline. TAOs have high expression levels in testis in mammals; however, the germline function of TAO kinase is not known in any system. The data presented here indicate that KIN-18 is required to coordinate recombination, oocyte differentiation, and apoptosis in the *C. elegans* germline. The absence of KIN-18 leads to accelerated recombination, ectopic oocyte differentiation, and elevated levels of apoptosis (summary in Figure 8). These results clearly support a meiotic role for TAO kinases in *C. elegans* oogenesis. We did not address the role of KIN-18 in spermatogenesis, which can also be affected by KIN-18.

KIN-18 is a molecular "timer," restricting MPK-1a activation to late pachytene nuclei

MPK-1 signaling is essential for meiotic progression and is under tight regulation by upstream kinases and phosphatases (Sundaram 2006). Our data suggest that KIN-18 regulates both the timing and the level of MPK-1 activation. Western blot analyses indicate that *kin-18* mutants have an increase in activated MPK-1a that is not due to changes in total protein levels; this suggests a role for KIN-18 as a negative regulator of MPK-1a activation. MPK-1a is required in the soma for vulva induction and was suggested to also be present in low levels in the germline [required for pachytene exit (Schouest *et al.* 2009)]. Thus, the increased levels of dpMPK-1a observed could be attributed to an increase in somatic dpMPK-1a activation, not necessarily occurring in the germline. Examination of dpMPK-1 in the germline via immunostaining and comparison of germline-deficient *kin-18* mutants reveal that dpMPK-1a regulation is indeed altered in the germline. dpMPK-1a localizes in an aberrant pattern in *kin-18* mutants ranging from no activation to multiple regions of activation, including premature activation. Furthermore, the *kin-18* mutant activation regions are not restricted to middle late pachytene where dpMPK-1a is normally observed. One interpretation of the data is that MPK-1 is activated in different regions in each gonad in *kin-18* mutants. Thus, while dpMPK-1 localization is variable between gonads, it remains "locked" in every gonad to a particular region (does not go through cycles of "on/off"). We believe that this is less likely, since if MPK-1 was constitutively activated in different regions in each germline, each *kin-18* mutant's gonad would have a distinct phenotype. However, we find the phenotype to be largely uniform. Alternatively, the variable pattern of staining observed in different gonads may reflect a "flickering" pattern of MPK-1a's activation, where each gonad analyzed represents a snapshot of the same biological outcome. If true, this "flickering" suggests that MPK-1a signaling in *kin-18* mutants is going through cycles and that the "on" state occurs at random and sometimes in multiple germline locations. Since the position of the nuclei in the germline reflects the time they spent in prophase, germline nuclei of *kin-18* mutants are exposed to MPK-1a signaling at the wrong time. Based on all the data above, we propose that KIN-18 regulates the timing of MPK-1a activation so that in wild-type MPK-1a can be activated only in middle–late pachytene nuclei around the bend region to facilitate apoptosis and oocyte differentiation. This model does not suggest that dpMPK-1

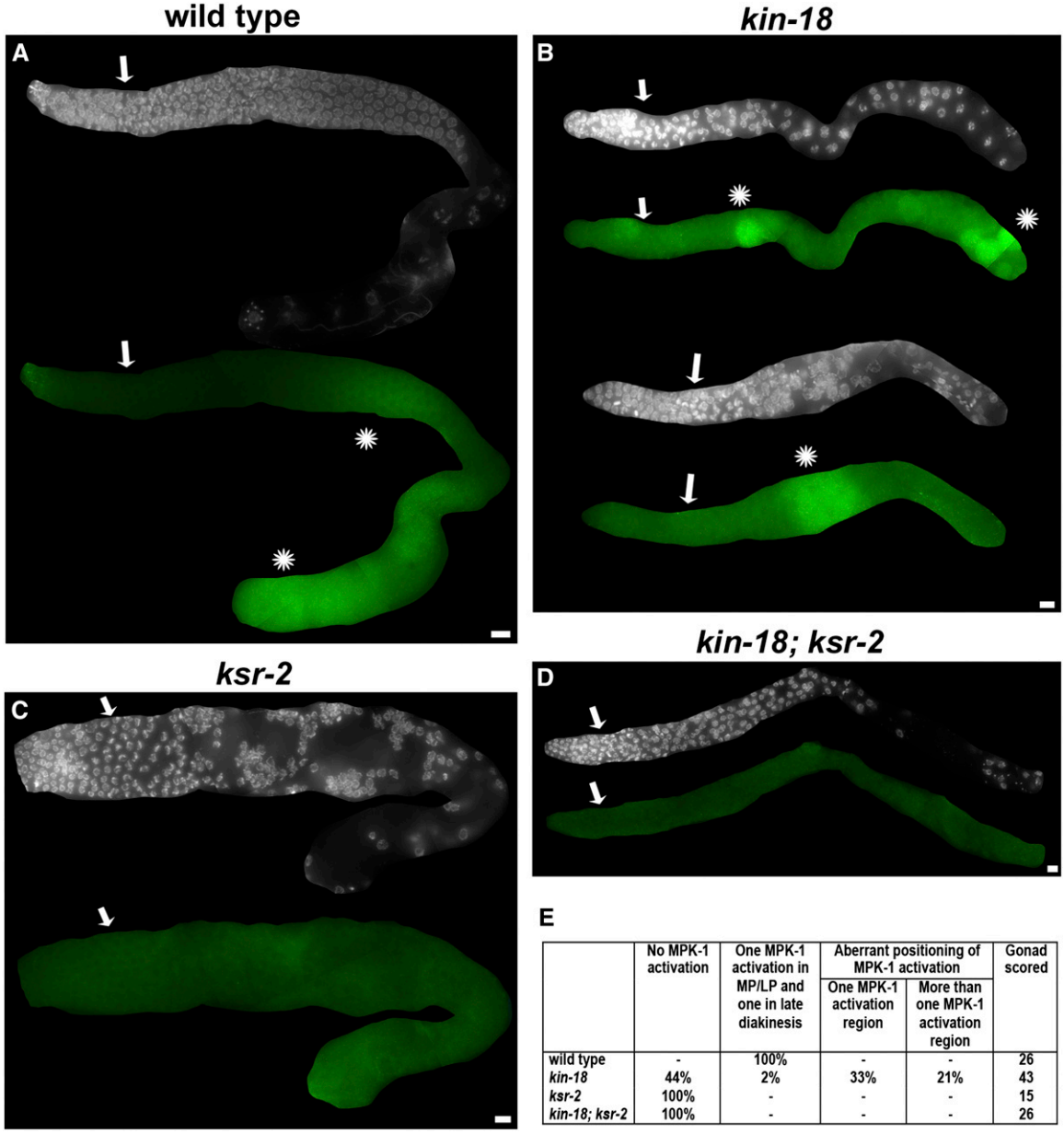

E

	No MPK-1 activation	One MPK-1 activation in MP/LP and one in late diakinesis	Aberrant positioning of MPK-1 activation		Gonad scored
			One MPK-1 activation region	More than one MPK-1 activation region	
wild type	-	100%	-	-	26
kin-18	44%	2%	33%	21%	43
ksr-2	100%	-	-	-	15
kin-18; ksr-2	100%	-	-	-	26

Figure 7 MPK-1 activation pattern is ectopic in *kin-18* mutants. Immunostaining of dpMPK-1 in (A) wild type, one gonad; (B) *kin-18*, two gonads; (C) *ksr-2*, one gonad; and (D) *ksr-2;kin-18*, one gonad. Each gonad is represented by two images of DAPI only (top) and double staining of dpMPK-1 and DAPI on the bottom. Images were not processed except that gonads were cropped from the whole image obtained. Wild type has two regions of MPK-1 activation. The *kin-18* mutants have an aberrant activation pattern. Activation is absent in *ksr-2* single and *kin-18;ksr-2* double mutants. (E) Number of gonads examined for wild type, *kin-18*, *ksr-2*, and *kin-18*; *ksr-2* in each one of the MPK-1 activation patterns indicated. Images are from a single panel and stitched by FIJI. Bar, 10 μm. White/blue, DAPI; green, dpMPK-1. Arrows represent first row with more than one clustered nuclei, as indication for meiotic entry. Asterisk represents MPK-1 activation zone.

phosphatase is also being simultaneously controlled by the KIN-18, but that there are multiple levels of control on dpMPK-1 ongoing and that some may not be under the control of KIN-18. In the absence of KIN-18, the "timer" of MPK-1 activation is lost and MPK-1a is activated at irregular times in germline development, leading to a "flickering" effect of MPK-1 signaling. This leads to defects in meiotic progression, which include ectopic oocyte apoptosis, which may prevent the expression of MPK-1b.

MPK-1 activation is essential for multiple aspects of meiotic progression

Activation of MPK-1 in late pachytene nuclei is crucial for maintaining a functional germline. Mutants that lack MPK-1 activation have a reduction in apoptosis, even under conditions in which apoptosis is induced by ionizing radiation (Rutkowski *et al.* 2011). Early MPK-1 activation can cause apoptosis in nuclei in which recombination has yet to be completed, leading to germ cell depletion. In *kin-18* mutants,

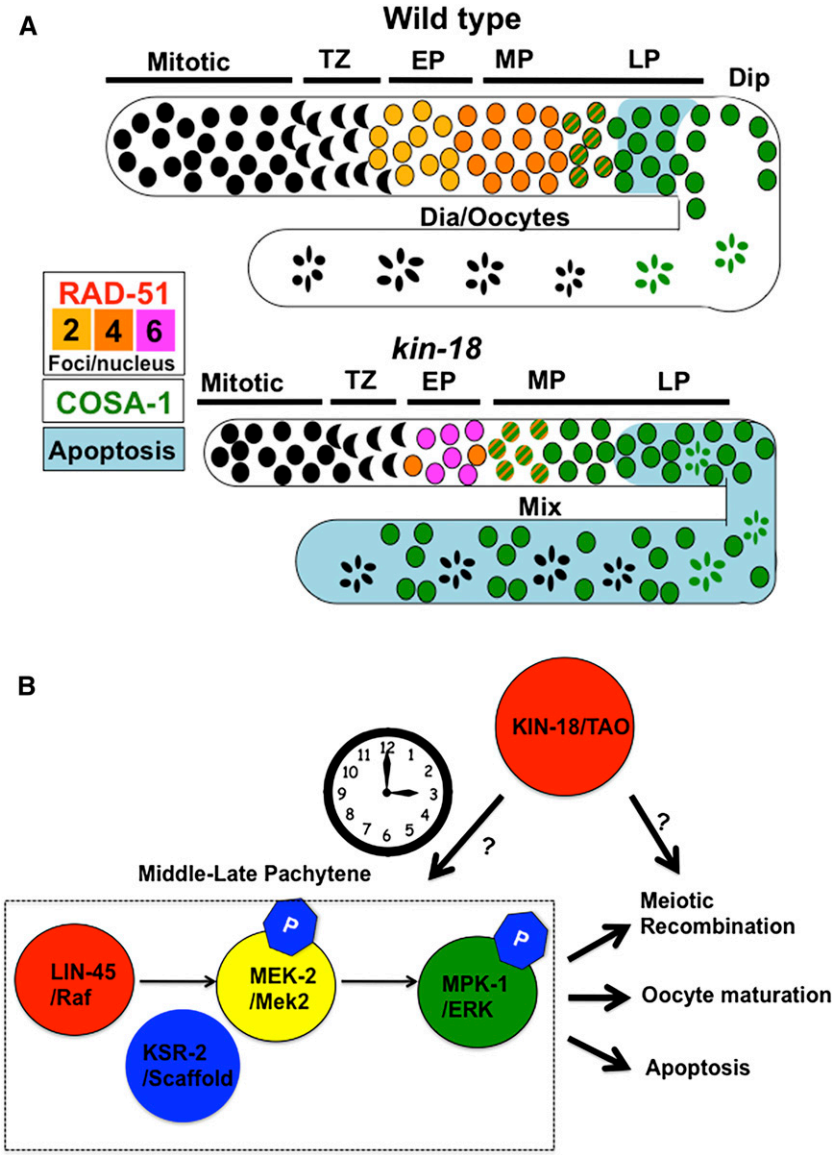

Figure 8 Summary of defects observed in *kin-18* mutants and a model for KIN-18 function. (A) Summary of defects observed in *kin-18* mutants: COSA-1 (green), RAD-51 (yellow, orange, and pink) and apoptosis (blue). MPK-1 is not represented here (due to variability of staining patterns in *kin-18* mutants). (B) Proposed model for KIN-18's role in meiosis. Arrows indicate positive regulation.

apoptosis levels are increased and some diakinesis nuclei appear in the distal regions in the germline (pre-bend), consistent with increased and ectopic MPK-1a activation. Oocytes produced by this aberrant meiosis are nonfunctional and cannot produce embryos, even when fertilized by wild-type sperm. In *kin-18* mutants, even diakinesis nuclei that show fully condensed (normal) chromosomal morphology are aberrant; they develop into small oocytes, abnormally disassemble the SC, abnormally localize PH3, and do not produce the germline-specific MPK-1b isoform. Disruption of normal MPK-1 activation also affects the overall number of germline nuclei, as mutants with enhanced MPK-1 activation [*lip-1*, *let-60(gf)* (Lee *et al.* 2006)] also exhibit fewer numbers of germline nuclei. This *kin-18* phenotype could be caused by the combination of elevated levels of apoptosis with reduced mitotic proliferation. Our data suggest that this reduction in nuclei number occurs mainly prior to apoptosis and therefore only partially depends on the elevated apoptosis caused by MPK-1 activation. These findings are consistent with the previously proposed potential role of MPK-1 signaling in mitotic proliferation (Lee *et al.* 2006, 2007).

MPK-1 signaling and the timing of meiotic DSB repair events

Meiotic recombination must be completed before germ cells differentiate into oocytes; there must be coordination between meiotic recombination and germline progression. MPK-1 signaling can be activated by DNA damage (ionizing irradiation), is involved in regulating DNA damage-induced apoptosis (Rutkowski *et al.* 2011), and was proposed to control the transition between RAD-50 dependent to independent loading of RAD-51 (Hayashi *et al.* 2007). Our work adds to these findings a possible link between MPK-1 signaling and DSB repair.

Although both loss of MPK-1 signaling (*ksr-2* mutants) and aberrant MPK-1 signaling (*kin-18* mutants) lead to an increase

in RAD-51 foci, they do not have the same effect on the timing of appearance of crossover markers (COSA-1). This leads us to propose that the nature of the recombination defects observed in *ksr-2* and *kin-18* mutants is distinct. Moreover, since *kin-18* is epistatic to *ksr-2* regarding both RAD-51 and COSA-1 foci analysis, the role that KIN-18 plays in recombination is likely not dependent on its effect on MPK-1 signaling. As a kinase, it is likely that the targets are more than one: one in the MPK-1 pathway, regulating late prophase events, and one, yet undetermined, regulating early recombination events.

How can recombination be affected differently by KIN-18 and KSR-2? RAD-51 is an ssDNA-binding protein that is required for recombination. Accumulation of early pachytene RAD-51 foci can be interpreted in one of two ways: either RAD-51 loads more quickly onto DNA or it has more difficulty unloading from DNA. The first scenario might be a result of accelerated processing of meiotic DSBs to form ssDNA, leading to earlier loading of RAD-51. The second scenario might reflect defects in the repair of DSBs, so that ssDNA persists longer due to delays in downstream steps of recombination. We cannot differentiate between these two models based merely on the analysis of RAD-51 foci numbers. However, combined analysis of RAD-51 and COSA-1 may help distinguish between the two possibilities. If ssDNA processing is accelerated, then DSBs should be more quickly repaired to form crossovers, which can be visualized as a premature appearance of COSA-1 foci (*i.e.*, *kin-18* mutants phenotype). However, if DSB repair is perturbed, COSA-1 will load with delayed or wild-type kinetics [depending on whether all crossovers or just non-interfering crossovers or gene conversions are targeted (*i.e.*, *ksr-2* mutants phenotype)]. In our model, KIN-18 does not regulate the number of DSBs or the crossover/noncrossover decision, but rather the kinetics/timing of recombination. As a result, the overall number of COSA-1 foci is not affected in the *kin-18* mutants. Our data are consistent with KIN-18 affecting earlier events in ssDNA processing that are upstream from KSR-2; however, in the absence of molecular data, this is, for now, only a working model.

It is possible that the elevated levels of RAD-51 in early pachytene are independent of MPK-1 signaling. However, KSR-2 is well studied, and the only known role for KSR-2 is in MPK-1 signaling. The effect of MPK-1 on DSB repair may be direct; among the many predicted targets of MPK-1 are two proteins required for homologous recombination repair of DSBs (RFS-1 and RPA-1) (Arur *et al.* 2009). If MPK-1 signaling indeed affects early pachytene events, how can early pachytene nuclei in *ksr-2* mutants exhibit alteration in the DNA damage repair pathway that is dependent on MPK-1 signaling, which is normally a mid-to-late pachytene event? This requires that early and mid-pachytene nuclei communicate. Despite the gonad being a syncytium, the germline is not uniform: protein and RNA distribution in the germline shows a gradient and directionality of information movement enforced by cytoplasmic streaming. However, the common cytoplasm potentially allows the exchange of information between nuclei, raising the possibility that nuclei are not completely autonomous. Signaling from MPK-1-activated nuclei (mid-pachytene) to DSB formation (early pachytene) may not be very challenging since these nuclei are positioned relatively close to each other. The idea that downstream meiotic events can affect early meiotic events is plausible based on recent findings; crossover formation or complete synapsis (a later meiotic event) can signal to affect the number of DSB formed (early meiotic event) (*e.g.*, Kauppi *et al.* 2013; Rosu *et al.* 2013). This model suggests that feedback loops communicate the progression of late meiotic events to regulate early meiotic events. The MPK-1-signaling pathway can be used to communicate such an effect in the *C. elegans* germline.

How does KIN-18 regulate MPK-1 activation in the germline?

We have shown that KIN-18 is required for the regulation of MPK-1a. The lack of MPK-1b protein can be explained by the aberrant oocyte differentiation and therefore is likely to be an indirect product of MPK-1a misregulation. The question of how KIN-18 regulates MPK-1a remains open. KIN-18 is unlikely to be a direct upstream kinase in the canonical MPK-1 cascade (LIN-45 → MEK-2 → MPK-1) or a kinase for the known MPK-1 phosphatase, LIP-1. First, if KIN-18 was a MAP3K of MPK-1a, lack of KIN-18 activity would eliminate MPK-1a phosphorylation. Since the opposite is true, KIN-18 likely does not regulate MPK-1a via MEK-2/MAPKK phosphorylation. Second, mutants of all genes known to directly activate/deactivate MPK-1 lead to phenotypes that differ from that of *kin-18* mutants (Church *et al.* 1995; Hajnal and Berset 2002; Hsu *et al.* 2002; Ohmachi *et al.* 2002). Third, mammalian TAO kinases can activate the JNK (MAPK)- and p38 (MAPK)-signaling cascade but not ERK (MAPK) (Hutchison *et al.* 1998; Chen *et al.* 1999; Yustein *et al.* 2003). Therefore, we propose that KIN-18 regulates MPK-1 activation in an indirect manner by the following two mechanisms. First, KIN-18 functions as a MAP3K that activates an unknown effector kinase to regulate the canonical MPK-1 signaling. In addition to the MPK-1 phosphatase, it has been reported that MPK-1 activation can be altered by a subset of its own targets potentially via a feedback loop (Arur *et al.* 2009). Therefore, one possibility could be that KIN-18 signaling also regulates some of the same targets that can alter the canonical MPK-1 pathway. Based on conservation of TAO kinases, it is possible that KIN-18 also activates p38 (MAPK) or JNK (MAPK) signaling to activate those targets in *C. elegans*. Nevertheless, viable mutants of p38 orthologs in *C. elegans* do not affect the germline; two JNK orthologs interact with P-granule proteins, making it difficult to dissect their specific function in JNK signaling (Berman *et al.* 2001a; Smith *et al.* 2002; Orsborn *et al.* 2007). Second, KIN-18 may function independently of its kinase activity by interacting with one of the proteins involved in the canonical MPK-1 cascade, preventing its activation. It has been shown *in vitro* that rat TAO kinase can bind another MAP3K, TAK1, to prevent TAK1 from activating one of its downstream targets

(Huangfu *et al.* 2006). While a wealth of evidence supports KIN-18's function as a MAP3K, KIN-18 was originally identified as a homolog of a MAP4K, Ste20p in *S. cerevisiae*, along with other Germline Center Kinases (GCKs). In *C. elegans*, a germline center kinase, GCK-1, shares homology with KIN-18 and exhibits a similar, yet not identical, set of germline phenotypes as *kin-18* mutants (Schouest *et al.* 2009). GCK-1 is speculated to regulate MPK-1 activation by sequestering MPK-1 protein, thus limiting its availability for activation (Schouest *et al.* 2009). It is possible that KIN-18 regulates MPK-1 activation utilizing a similar mechanism. Future investigations of potential targets as well as localization of KIN-18 would shed light onto the mechanism of KIN-18 regulation of MPK-1 signaling.

Based on our analysis of KIN-18 function in the *C. elegans* germline, it is likely that TAO kinases participate in germline development in other organisms as well. This is consistent with the high levels of germline expression of TAO kinase in rat and human testis (Hutchison *et al.* 1998; Yustein *et al.* 2003). Moreover, work in tissue culture has established a role for TAO kinase in the DNA damage-signaling response. DNA damage induced by ionizing radiation induces TAO2 expression, and TAOs are required for p38-mediated cell cycle arrest following ionizing radiation (Raman *et al.* 2007). We have shown that KIN-18's effect on MPK-1 signaling affects the timely progression of recombination in meiosis. Our studies may therefore offer a way to understand the role that TAO kinases play in the germline of higher eukaryotes: coordinating key events such as recombination and apoptosis with meiotic progression.

Acknowledgments

Some strains were provided by the Caenorhabditis Genome Center, which is funded by National Institutes of Health Office of Research Infrastructure Programs (P40-OD010440). We thank M. Zetka for HIM-3 and HTP-3 antibodies; J. Kimble for the GLD-1 antibody; D. Houston for his help with membrane-staining reagents; V. Prahlad, R. E. Malone, and members of the Smolikove lab for critical reading of this manuscript; R. E. Malone and A. Wickenkamp for their help in sharing unpublished work that cultivated our interest in KIN-18; and R. E. Malone for discussion of our data. This work was supported mainly by National Science Foundation grant MCB-1121150 (to S.S.) and in part by National Institutes of Health grant R01GM112657 (to S.S.).

Literature Cited

Alpi, A., P. Pasierbek, A. Gartner, and J. Loidl, 2003 Genetic and cytological characterization of the recombination protein RAD-51 in Caenorhabditis elegans. Chromosoma 112: 6–16.

Andux, S., and R. E. Ellis, 2008 Apoptosis maintains oocyte quality in aging Caenorhabditis elegans females. PLoS Genet. 4: e1000295.

Arur, S., M. Ohmachi, S. Nayak, M. Hayes, A. Miranda *et al.*, 2009 Multiple ERK substrates execute single biological processes in Caenorhabditis elegans germ-line development. Proc. Natl. Acad. Sci. USA 106: 4776–4781.

Berman, K., J. McKay, L. Avery, and M. Cobb, 2001a Isolation and characterization of pmk-(1–3): three p38 homologs in Caenorhabditis elegans. Mol. Cell Biol. Res. Commun. 4: 337–344.

Berman, K. S., M. Hutchison, L. Avery, and M. H. Cobb, 2001b kin-18, a C. elegans protein kinase involved in feeding. Gene 279: 137–147.

Brenner, S., 1974 The genetics of *Caenorhabditis elegans*. Genetics 77: 71–94.

Brockway, H., N. Balukoff, M. Dean, B. Alleva, and S. Smolikove, 2014 The CSN/COP9 signalosome regulates synaptonemal complex assembly during meiotic prophase I of Caenorhabditis elegans. PLoS Genet. 10: e1004757.

Chen, Z., and M. H. Cobb, 2001 Regulation of stress-responsive mitogen-activated protein (MAP) kinase pathways by TAO2. J. Biol. Chem. 276: 16070–16075.

Chen, Z., M. Hutchison, and M. H. Cobb, 1999 Isolation of the protein kinase TAO2 and identification of its mitogen-activated protein kinase/extracellular signal-regulated kinase kinase binding domain. J. Biol. Chem. 274: 28803–28807.

Chen, Z., M. Raman, L. Chen, S. F. Lee, A. G. Gilman *et al.*, 2003 TAO (thousand-and-one amino acid) protein kinases mediate signaling from carbachol to p38 mitogen-activated protein kinase and ternary complex factors. J. Biol. Chem. 278: 22278–22283.

Church, D. L., K. L. Guan, and E. J. Lambie, 1995 Three genes of the MAP kinase cascade, mek-2, mpk-1/sur-1 and let-60 ras, are required for meiotic cell cycle progression in Caenorhabditis elegans. Development 121: 2525–2535.

Cole, F., L. Kauppi, J. Lange, I. Roig, R. Wang *et al.*, 2012 Homeostatic control of recombination is implemented progressively in mouse meiosis. Nat. Cell Biol. 14: 424–430.

Crittenden, S. L., K. A. Leonhard, D. T. Byrd, and J. Kimble, 2006 Cellular analyses of the mitotic region in the Caenorhabditis elegans adult germ line. Mol. Biol. Cell 17: 3051–3061.

Dernburg, A. F., K. McDonald, G. Moulder, R. Barstead, M. Dresser *et al.*, 1998 Meiotic recombination in C. elegans initiates by a conserved mechanism and is dispensable for homologous chromosome synapsis. Cell 94: 387–398.

Fan, H. Y., and Q. Y. Sun, 2004 Involvement of mitogen-activated protein kinase cascade during oocyte maturation and fertilization in mammals. Biol. Reprod. 70: 535–547.

Gartner, A., P. R. Boag, and T. K. Blackwell, 2008 Germline Survival and Apoptosis (September 4, 2008), WormBook, ed. The C. elegans Research Community, WormBook, doi/10.1895/wormbook.1.145.1, http://www.wormbook.org.

Gumienny, T. L., E. Lambie, E. Hartwieg, H. R. Horvitz, and M. O. Hengartner, 1999 Genetic control of programmed cell death in the Caenorhabditis elegans hermaphrodite germline. Development 126: 1011–1022.

Hajnal, A., and T. Berset, 2002 The C.elegans MAPK phosphatase LIP-1 is required for the G(2)/M meiotic arrest of developing oocytes. EMBO J. 21: 4317–4326.

Hayashi, M., G. M. Chin, and A. M. Villeneuve, 2007 C. elegans germ cells switch between distinct modes of double-strand break repair during meiotic prophase progression. PLoS Genet. 3: e191.

Hsu, V., C. L. Zobel, E. J. Lambie, T. Schedl, and K. Kornfeld, 2002 *Caenorhabditis elegans* lin-45 raf is essential for larval viability, fertility and the induction of vulval cell fates. Genetics 160: 481–492.

Huangfu, W. C., E. Omori, S. Akira, K. Matsumoto, and J. Ninomiya-Tsuji, 2006 Osmotic stress activates the TAK1-JNK pathway while blocking TAK1-mediated NF-kappaB activation: TAO2 regulates TAK1 pathways. J. Biol. Chem. 281: 28802–28810.

Hutchison, M., K. S. Berman, and M. H. Cobb, 1998 Isolation of TAO1, a protein kinase that activates MEKs in stress-activated protein kinase cascades. J. Biol. Chem. 273: 28625–28632.

Kauppi, L., M. Barchi, J. Lange, F. Baudat, M. Jasin *et al.*, 2013 Numerical constraints and feedback control of double-strand breaks in mouse meiosis. Genes Dev. 27: 873–886.

Keeney, S., C. N. Giroux, and N. Kleckner, 1997 Meiosis-specific DNA double-strand breaks are catalyzed by Spo11, a member of a widely conserved protein family. Cell 88: 375–384.

Kelly, K. O., A. F. Dernburg, G. M. Stanfield, and A. M. Villeneuve, 2000 *Caenorhabditis elegans msh-5* is required for both normal and radiation-induced meiotic crossing over but not for completion of meiosis. Genetics 156: 617–630.

Kosinski, M., K. McDonald, J. Schwartz, I. Yamamoto, and D. Greenstein, 2005 C. elegans sperm bud vesicles to deliver a meiotic maturation signal to distant oocytes. Development 132: 3357–3369.

Lee, M. H., B. Hook, L. B. Lamont, M. Wickens, and J. Kimble, 2006 LIP-1 phosphatase controls the extent of germline proliferation in Caenorhabditis elegans. EMBO J. 25: 88–96.

Lee, M. H., M. Ohmachi, S. Arur, S. Nayak, R. Francis *et al.*, 2007 Multiple functions and dynamic activation of MPK-1 extracellular signal-regulated kinase signaling in *Caenorhabditis elegans* germline development. Genetics 177: 2039–2062.

Lopez, A. L. III, J. Chen, H. J. Joo, M. Drake, M. Shidate *et al.*, 2013 DAF-2 and ERK couple nutrient availability to meiotic progression during Caenorhabditis elegans oogenesis. Dev. Cell 27: 227–240.

MacQueen, A. J., M. P. Colaiacovo, K. McDonald, and A. M. Villeneuve, 2002 Synapsis-dependent and -independent mechanisms stabilize homolog pairing during meiotic prophase in C. elegans. Genes Dev. 16: 2428–2442.

Martin, J. S., N. Winkelmann, M. I. Petalcorin, M. J. McIlwraith, and S. J. Boulton, 2005 RAD-51-dependent and -independent roles of a Caenorhabditis elegans BRCA2-related protein during DNA double-strand break repair. Mol. Cell. Biol. 25: 3127–3139.

Miller, M. A., V. Q. Nguyen, M. H. Lee, M. Kosinski, T. Schedl *et al.*, 2001 A sperm cytoskeletal protein that signals oocyte meiotic maturation and ovulation. Science 291: 2144–2147.

Moore, T. M., R. Garg, C. Johnson, M. J. Coptcoat, A. J. Ridley *et al.*, 2000 PSK, a novel STE20-like kinase derived from prostatic carcinoma that activates the c-Jun N-terminal kinase mitogen-activated protein kinase pathway and regulates actin cytoskeletal organization. J. Biol. Chem. 275: 4311–4322.

Nabeshima, K., A. M. Villeneuve, and M. P. Colaiacovo, 2005 Crossing over is coupled to late meiotic prophase bivalent differentiation through asymmetric disassembly of the SC. J. Cell Biol. 168: 683–689.

Ohmachi, M., C. E. Rocheleau, D. Church, E. Lambie, T. Schedl *et al.*, 2002 C. elegans ksr-1 and ksr-2 have both unique and redundant functions and are required for MPK-1 ERK phosphorylation. Curr. Biol. 12: 427–433.

Orsborn, A. M., W. Li, T. J. McEwen, T. Mizuno, E. Kuzmin *et al.*, 2007 GLH-1, the C. elegans P granule protein, is controlled by the JNK KGB-1 and by the COP9 subunit CSN-5. Development 134: 3383–3392.

Pearson, G., F. Robinson, T. Beers Gibson, B. E. Xu, M. Karandikar *et al.*, 2001 Mitogen-activated protein (MAP) kinase pathways: regulation and physiological functions. Endocr. Rev. 22: 153–183.

Qiao, H., H. B. Prasada Rao, Y. Yang, J. H. Fong, J. M. Cloutier *et al.*, 2014 Antagonistic roles of ubiquitin ligase HEI10 and SUMO ligase RNF212 regulate meiotic recombination. Nat. Genet. 46: 194–199.

Raman, M., S. Earnest, K. Zhang, Y. Zhao, and M. H. Cobb, 2007 TAO kinases mediate activation of p38 in response to DNA damage. EMBO J. 26: 2005–2014.

Rosu, S., K. A. Zawadzki, E. L. Stamper, D. E. Libuda, A. L. Reese *et al.*, 2013 The C. elegans DSB-2 protein reveals a regulatory network that controls competence for meiotic DSB formation and promotes crossover assurance. PLoS Genet. 9: e1003674.

Rutkowski, R., R. Dickinson, G. Stewart, A. Craig, M. Schimpl *et al.*, 2011 Regulation of Caenorhabditis elegans p53/CEP-1-dependent germ cell apoptosis by Ras/MAPK signaling. PLoS Genet. 7: e1002238.

Schild-Prufert, K., T. T. Saito, S. Smolikov, Y. Gu, M. Hincapie *et al.*, 2011 Organization of the synaptonemal complex during meiosis in *Caenorhabditis elegans*. Genetics 189: 411–421.

Schouest, K. R., Y. Kurasawa, T. Furuta, N. Hisamoto, K. Matsumoto *et al.*, 2009 The germinal center kinase GCK-1 is a negative regulator of MAP kinase activation and apoptosis in the C. elegans germline. PLoS One 4: e7450.

Schvarzstein, M., S. M. Wignall, and A. M. Villeneuve, 2010 Coordinating cohesion, co-orientation, and congression during meiosis: lessons from holocentric chromosomes. Genes Dev. 24: 219–228.

Smith, P., W. M. Leung-Chiu, R. Montgomery, A. Orsborn, K. Kuznicki *et al.*, 2002 The GLH proteins, Caenorhabditis elegans P granule components, associate with CSN-5 and KGB-1, proteins necessary for fertility, and with ZYX-1, a predicted cytoskeletal protein. Dev. Biol. 251: 333–347.

Spiga, F. M., M. Prouteau, and M. Gotta, 2013 The TAO kinase KIN-18 regulates contractility and establishment of polarity in the C. elegans embryo. Dev. Biol. 373: 26–38.

Sundaram, M. V., 2006 RTK/Ras/MAPK signaling (February 11, 2006), WormBook, ed. The C. elegans Research Community, WormBook, doi/10.1895/wormbook.1.80.1, http://www.wormbook.org.

Widmann, C., S. Gibson, M. B. Jarpe, and G. L. Johnson, 1999 Mitogen-activated protein kinase: conservation of a three-kinase module from yeast to human. Physiol. Rev. 79: 143–180.

Yin, Y., and S. Smolikove, 2013 Impaired resection of meiotic double-strand breaks channels repair to nonhomologous end joining in Caenorhabditis elegans. Mol. Cell. Biol. 33: 2732–2747.

Yokoo, R., K. A. Zawadzki, K. Nabeshima, M. Drake, S. Arur *et al.*, 2012 COSA-1 reveals robust homeostasis and separable licensing and reinforcement steps governing meiotic crossovers. Cell 149: 75–87.

Yustein, J. T., L. Xia, J. M. Kahlenburg, D. Robinson, D. Templeton *et al.*, 2003 Comparative studies of a new subfamily of human Ste20-like kinases: homodimerization, subcellular localization, and selective activation of MKK3 and p38. Oncogene 22: 6129–6141.

Zickler, D., and N. Kleckner, 1999 Meiotic chromosomes: integrating structure and function. Annu. Rev. Genet. 33: 603–754.

Zou, W., Q. Lu, D. Zhao, W. Li, J. Mapes *et al.*, 2009 Caenorhabditis elegans myotubularin MTM-1 negatively regulates the engulfment of apoptotic cells. PLoS Genet. 5: e1000679.

Communicating editor: M. P. Colaiácovo

GENETICS

Supporting Information
www.genetics.org/lookup/suppl/doi:10.1534/genetics.115.177295/-/DC1

Coordination of Recombination with Meiotic Progression in the *Caenorhabditis elegans* Germline by KIN-18, a TAO Kinase That Regulates the Timing of MPK-1 Signaling

Yizhi Yin, Sean Donlevy, and Sarit Smolikove

DOI: 10.1534/genetics.115.177295

Figure S1

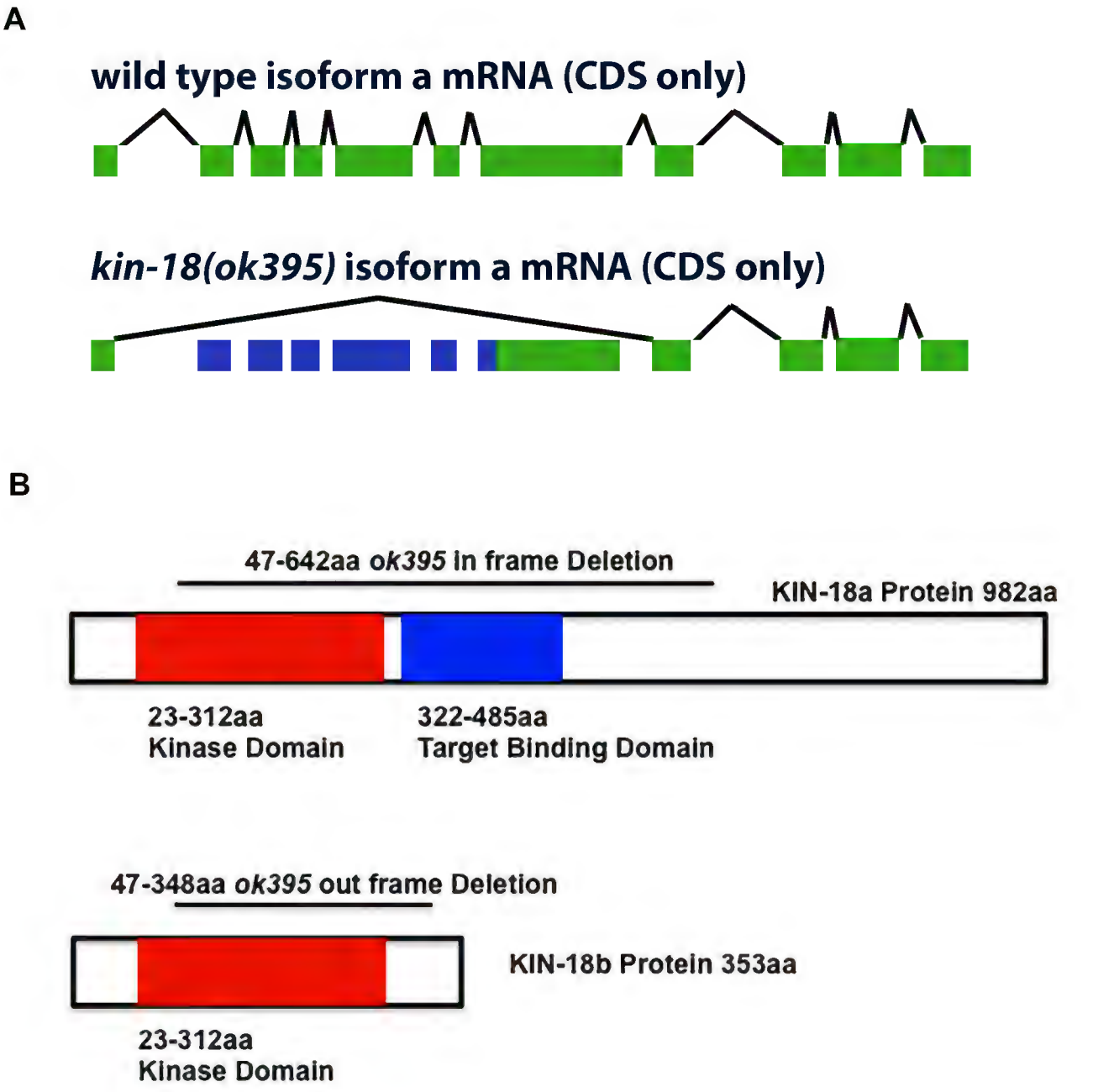
A
wild type isoform a mRNA (CDS only)
kin-18(ok395) isoform a mRNA (CDS only)
B
47-642aa ok395 in frame Deletion
KIN-18a Protein 982aa
23-312aa
Kinase Domain
322-485aa
Target Binding Domain
47-348aa ok395 out frame Deletion
KIN-18b Protein 353aa
23-312aa
Kinase Domain

Figure S2

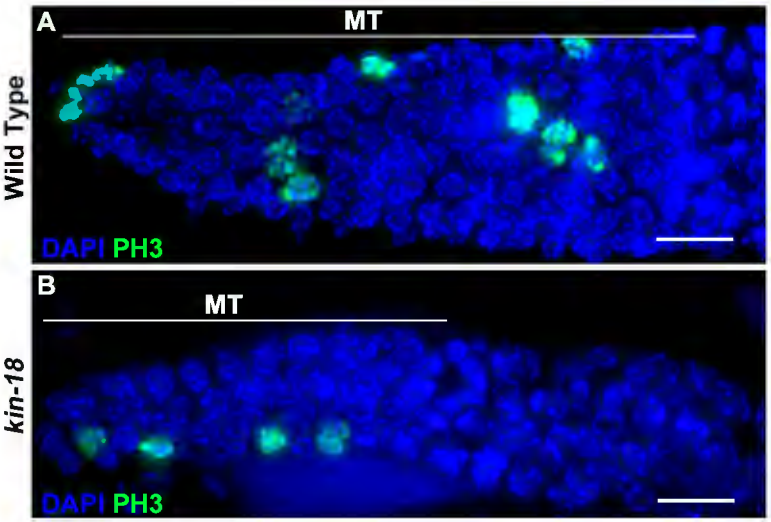

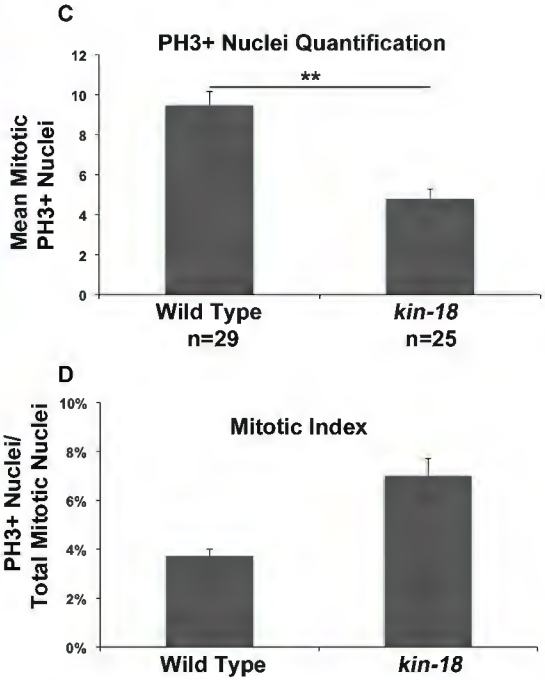

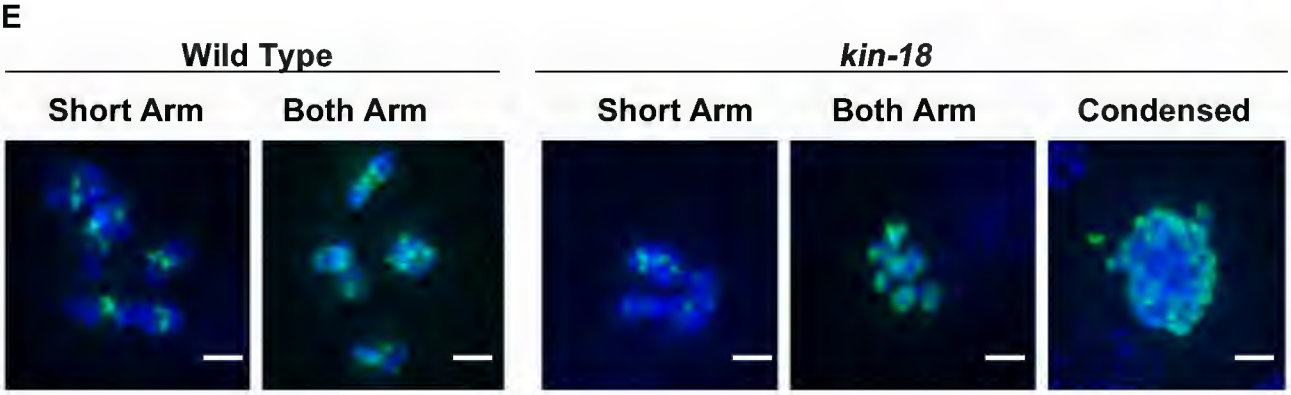

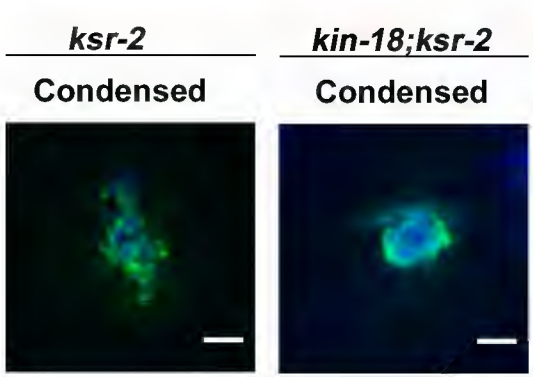

F

Genotype	# Gonads no PH3	# Gonads with PH3	#Short arm PH3 Oocyte	#Both arm PH3 Oocyte	# PH3 – Condensed
Wild Type	0 (0.0%)	25 (100%)	51	5	0
kin-18	21 (41.2%)	30 (58.8%)	5	22**	27
ksr-2	10 (83.3%)	2 (16.7%)	0	0	2
kin-18;ksr-2	23 (92.0%)	2 (8.0%)	0	0	2

Figure S3

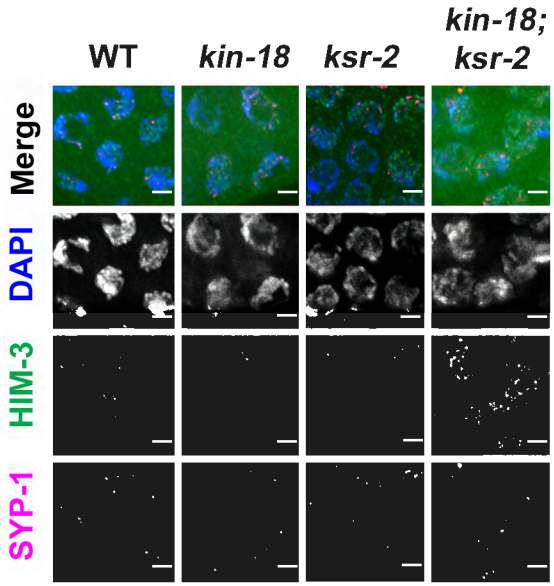

Figure S4

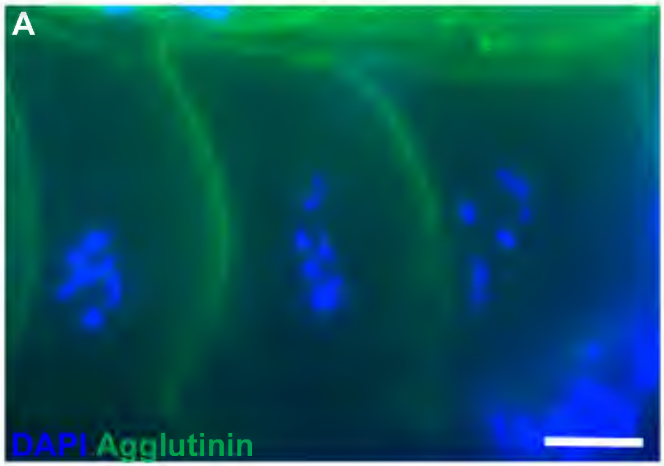
A
Wild Type
DAPI Agglutinin

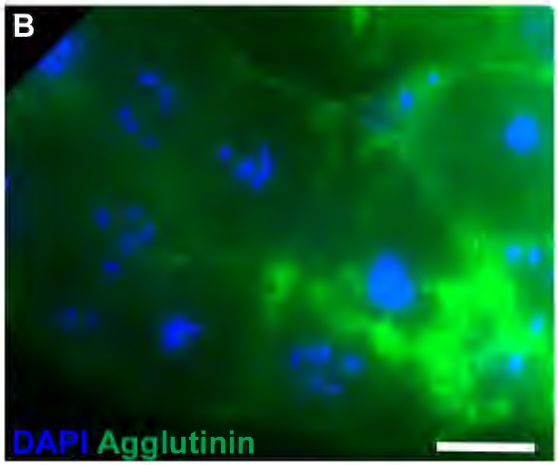
B
kin-18
DAPI Agglutinin

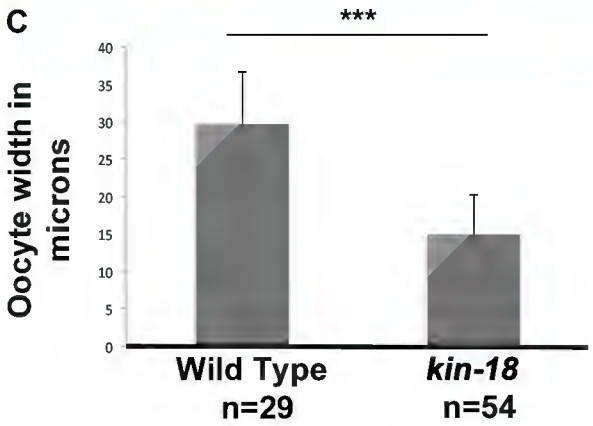
C
***
Oocyte width in microns
40
35
30
25
20
15
10
5
0
Wild Type
n=29
kin-18
n=54

Figure S5

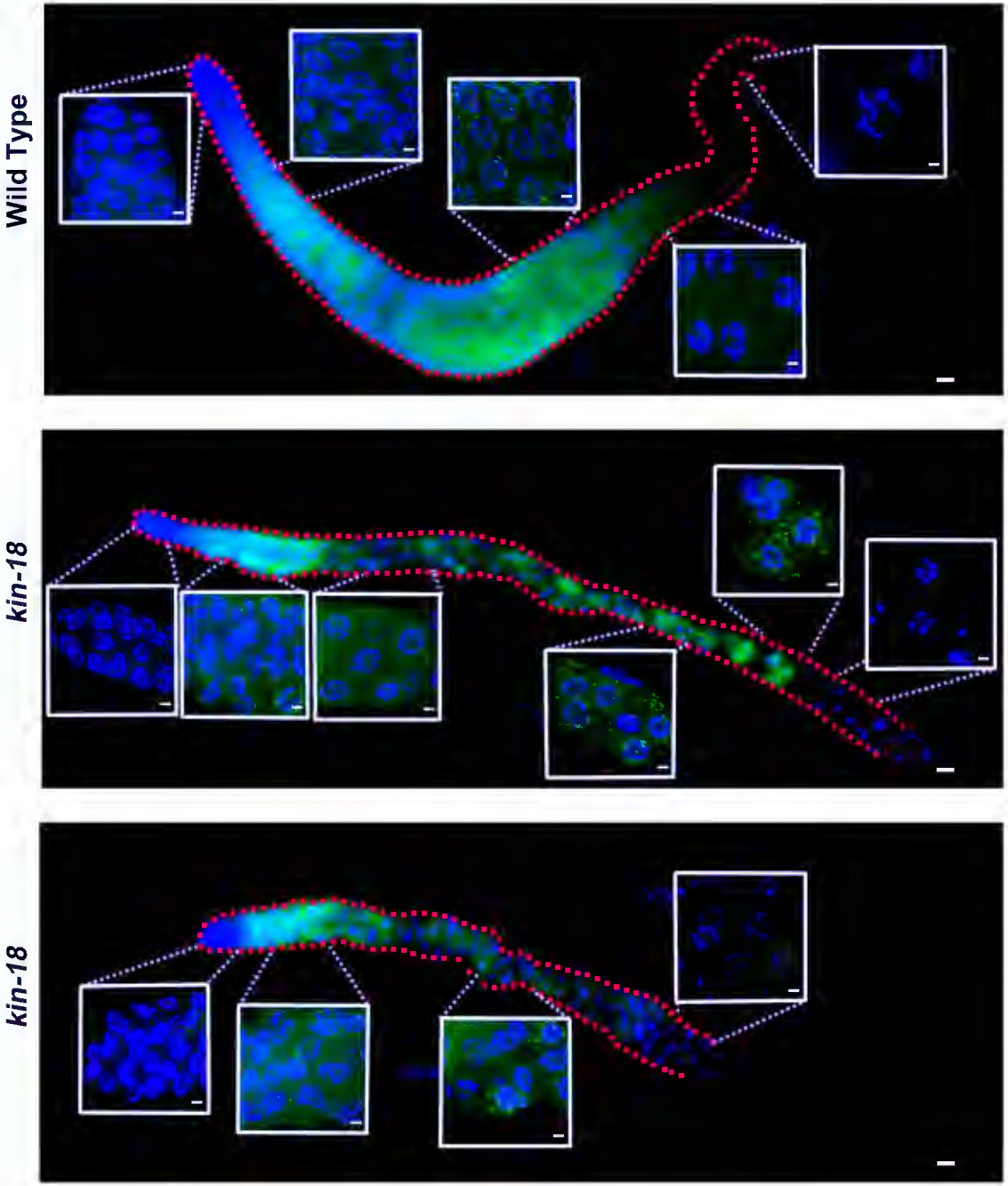

Figure S6

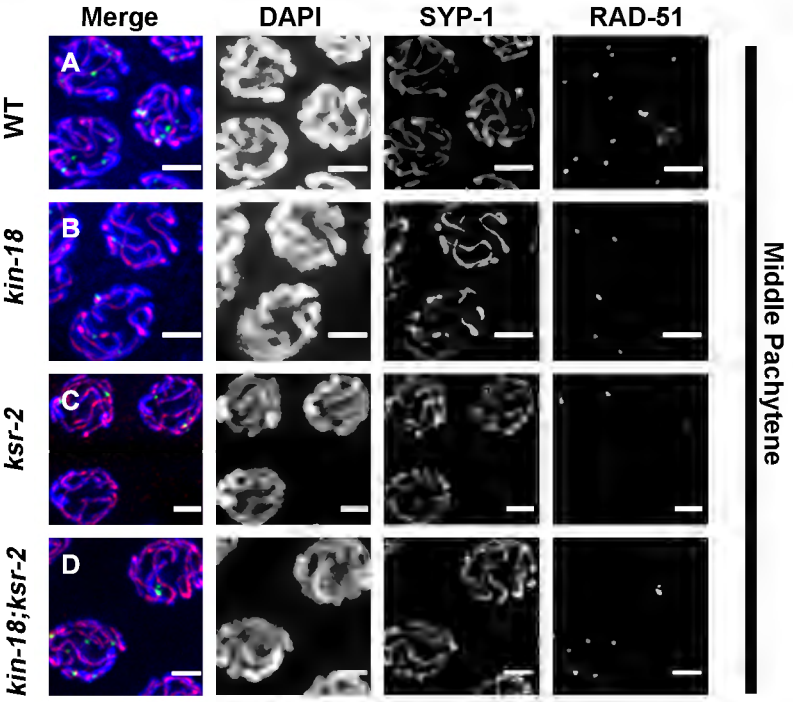
Merge
DAPI
SYP-1
RAD-51
A
WT
B
kin-18
C
ksr-2
D
kin-18;ksr-2
Middle Pachytene

Figure S7

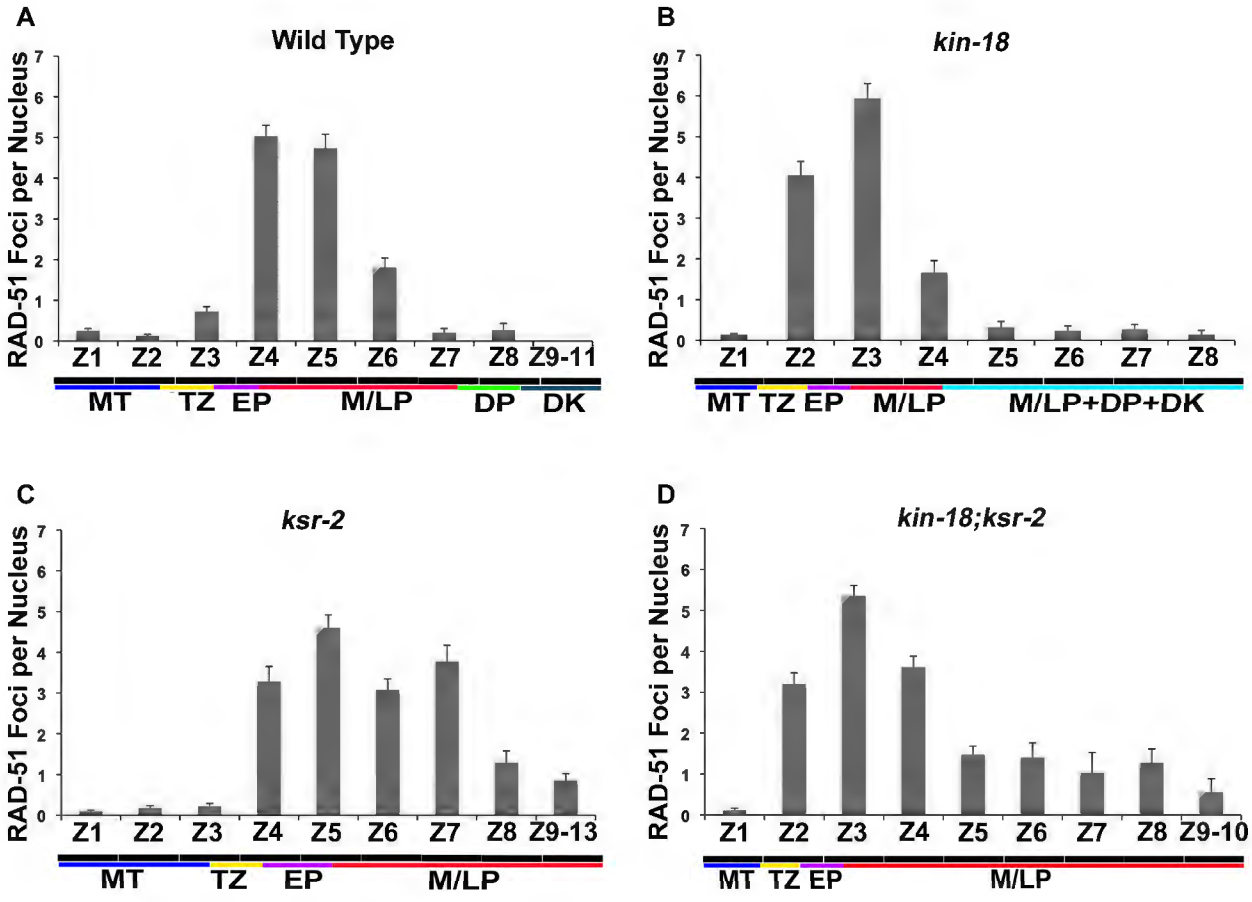
A
Wild Type
RAD-51 Foci per Nucleus
0
1
2
3
4
5
6
7
Z1
Z2
Z3
Z4
Z5
Z6
Z7
Z8
Z9-11
MT
TZ
EP
M/LP
DP
DK
B
kin-18
RAD-51 Foci per Nucleus
Z1
Z2
Z3
Z4
Z5
Z6
Z7
Z8
MT
TZ
EP
M/LP
M/LP+DP+DK
C
ksr-2
RAD-51 Foci per Nucleus
Z1
Z2
Z3
Z4
Z5
Z6
Z7
Z8
Z9-13
MT
TZ
EP
M/LP
D
kin-18;ksr-2
RAD-51 Foci per Nucleus
Z1
Z2
Z3
Z4
Z5
Z6
Z7
Z8
Z9-10
MT
TZ
EP
M/LP

Figure S8

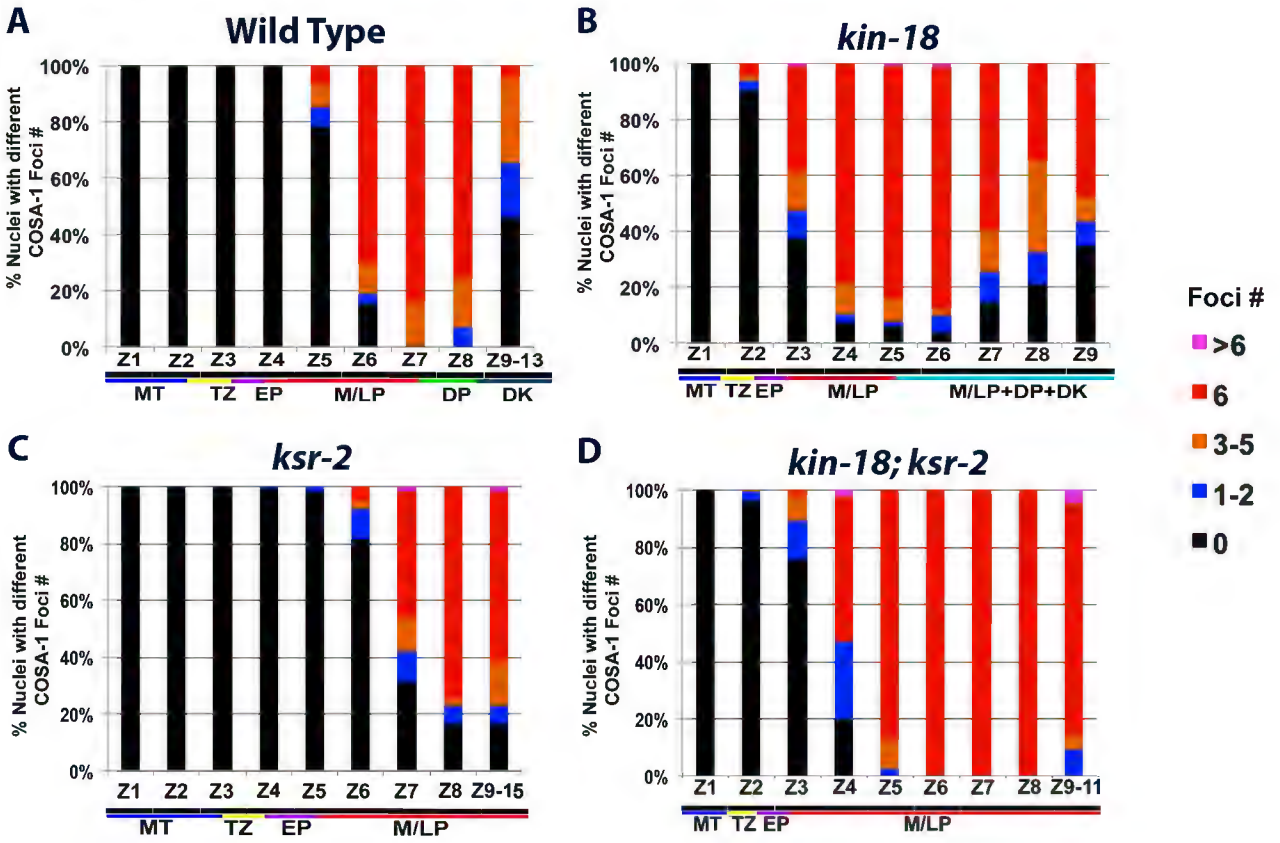
A
Wild Type
% Nuclei with different COSA-1 Foci #
100%
80%
60%
40%
20%
0%
Z1 Z2 Z3 Z4 Z5 Z6 Z7 Z8 Z9-13
MT TZ EP M/LP DP DK
B
kin-18
% Nuclei with different COSA-1 Foci #
100%
80%
60%
40%
20%
0%
Z1 Z2 Z3 Z4 Z5 Z6 Z7 Z8 Z9
MT TZ EP M/LP M/LP+DP+DK
C
ksr-2
% Nuclei with different COSA-1 Foci #
100%
80%
60%
40%
20%
0%
Z1 Z2 Z3 Z4 Z5 Z6 Z7 Z8 Z9-15
MT TZ EP M/LP
D
kin-18; ksr-2
% Nuclei with different COSA-1 Foci #
100%
80%
60%
40%
20%
0%
Z1 Z2 Z3 Z4 Z5 Z6 Z7 Z8 Z9-11
MT TZ EP M/LP
Foci #
>6
6
3-5
1-2
0

Figure S9

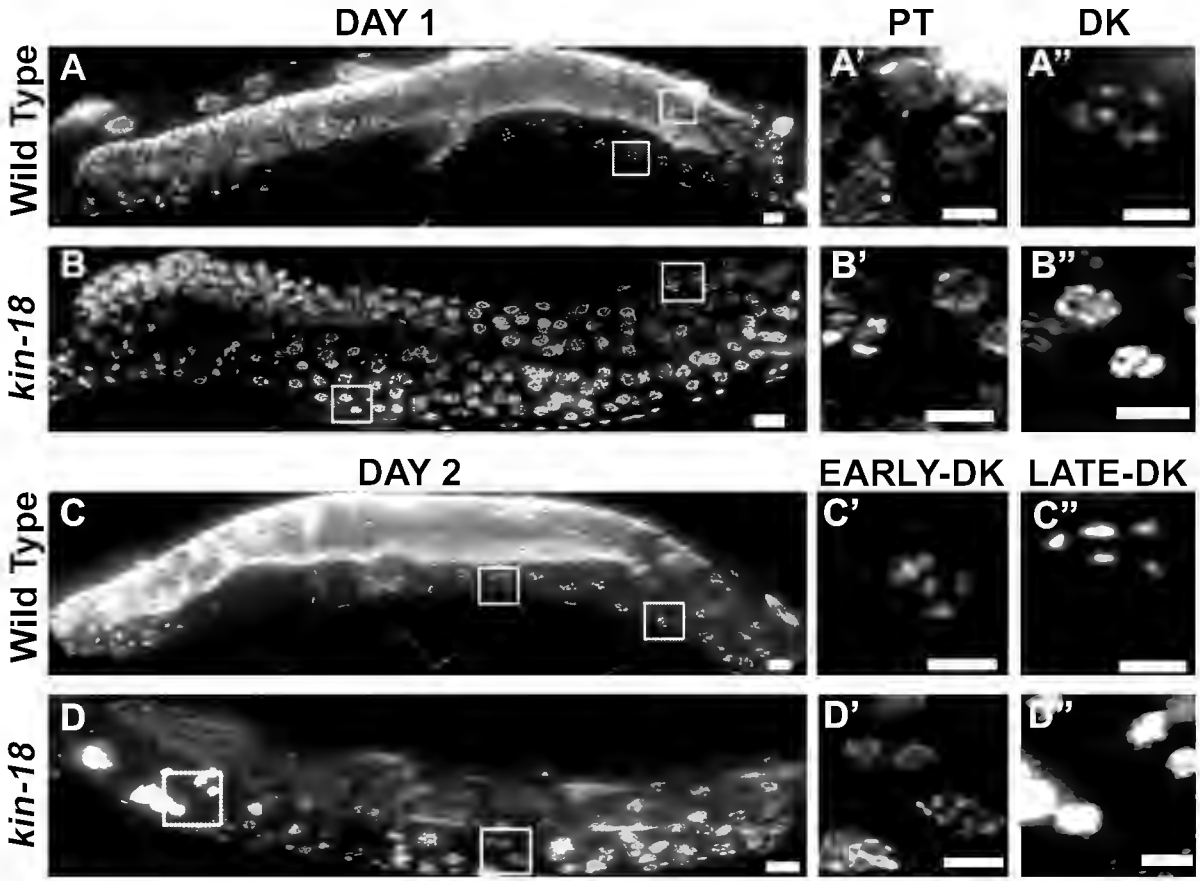
DAY 1
PT
DK
Wild Type
A
A'
A''
kin-18
B
B'
B''
DAY 2
EARLY-DK
LATE-DK
Wild Type
C
C'
C''
kin-18
D
D'
D''

Figure S10

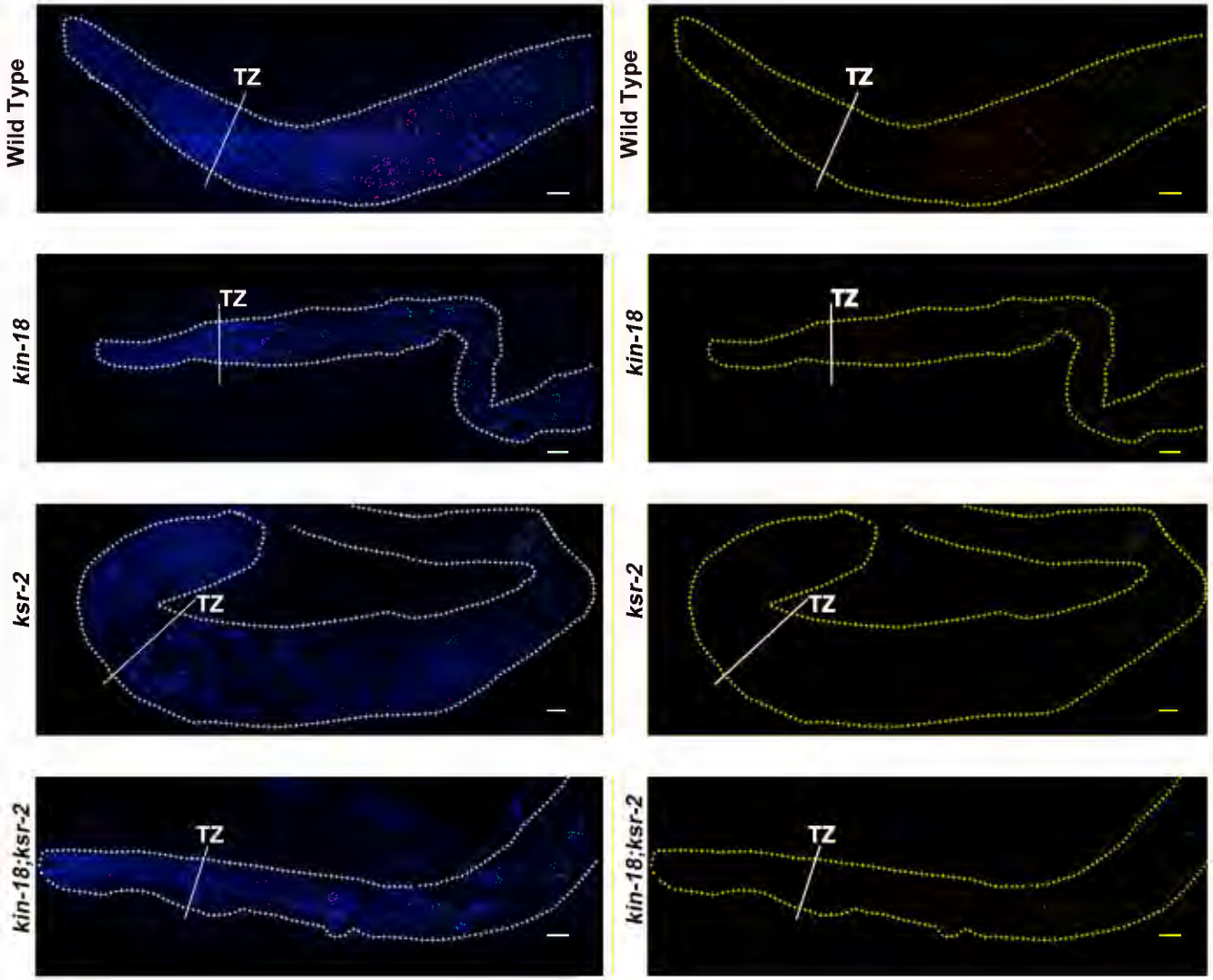
Wild Type
TZ
Wild Type
TZ
kin-18
TZ
kin-18
TZ
ksr-2
TZ
ksr-2
TZ
kin-18;ksr-2
TZ
kin-18;ksr-2
TZ
DAPI RAD-51 COSA-1

Table S1. The average number and percentage of nuclei in different meiotic stages

Type	MT	TZ	EP	M/LP	DP/DK	Others*	Total
Wild Type	250.6±13.3 (36.5±1.3%)	84.0±8.6 (12.3±1.2%)	98.2±8.0 (14.5±1.6%)	241.4±30.6 (34.8±3.2%)	12.4±1.4 (1.8±0.2%)	0.4±0.2 (0.1±0.03%)	687.0±34.1 (n=5)
kin-18	68.4±2.6 (30.7±1.4%)	17.0±1.8 (7.6±0.7%)	33.4±3.7 (14.9±1.6%)	93.6±6.0 (41.7±5.0%)	9.0±1.4 (4.1±0.7%)	2.0±0.4 (0.9±0.2%)	223.4±7.1 (n=7)
ksr-2	252.8±20 (39.9±2.7%)	90.4±16 (14.4±2.6%)	76.2±14 (11.9±2.0%)	208.2±6.2 (33.0±1.2%)	0.4±0.4 (0.1±0.1%)	3.2±1.2 (0.5±0.2%)	631.2±14.5 (n=5)
kin-18;ksr-2	85.4±9.1 (31.5±2.0%)	29.4±3.6 (11.2±1.6)	36.7±5.6 (13.9±2.4%)	116.4±1.5 (43.1±3.3%)	0.3±0.2 (0.1±0.1%)	0.7±0.3 (0.3±0.1%)	269.0±15.3 (n=7)

Number and percentage of nuclei at different meiotic stage are presented as Average±SE (Average±SE%). Others include apoptotic nuclei, condensed or loose DAPI bodies that do not resemble nuclei from any meiotic stage. n=# of gonads scored.

Table S2 The p values of nuclei in different meiotic stages

Type	Wild Type	*kin-18*	*ksr-2*	Stage
kin-18	p<0.001			Mitotic Tip
ksr-2	p<0.01	p<0.001		
kin-18;ksr-2	p<0.001	p>0.05	p<0.001	
Type	Wild Type	*kin-18*	*ksr-2*	Stage
kin-18	p<0.001			Transition Zone
ksr-2	p<0.05	p<0.001		
kin-18;ksr-2	p>0.05	p<0.001	p<0.001	

Type	Wild Type	*kin-18*	*ksr-2*	Stage
kin-18	p >0.05			Early Pachytene
ksr-2	p<0.01	p<0.01		
kin-18;ksr-2	p >0.05	p >0.05	p >0.05	
Type	Wild Type	*kin-18*	*ksr-2*	Stage
kin-18	p<0.001			Middle/Late Pachytene
ksr-2	p >0.05	p<0.001		
kin-18;ksr-2	p<0.001	p >0.05	p<0.001	

Type	Wild Type	*kin-18*	*ksr-2*	Stage
kin-18	p<0.001			Diplotene + Diakinesis
ksr-2	p<0.001	p<0.001		
kin-18;ksr-2	p<0.001	p<0.001	p >0.05	

Two tailed Fisher's exact test were performed at 95% C. I.

Table S3. Number of diakinesis oocytes with wild type and aberrant SYP-1 morphology

	Wild Type SYP-1	Aberrant SYP-1
WT	30	0
*kin-18***	0	20
ksr-2	NA	NA
kin-18;ksr-2	2	0

**p<0.001 Two tailed Fisher's exact test at 95% C.I. compared to wild type.

Table S4. The average RAD-51 foci in each meiotic stage

Type	MT	TZ	EP	M/LP	DP/DK
wild type	0.20±0.03, n=301	0.25±0.05, n=159	2.35±0.25, n=107	3.85±0.19, n=330	0.08±0.05, n=56
kin-18	0.15±0.02, n=324	0.30±0.10, n=152	6.99±0.47, n=143	2.79±0.18, n=450	0.07±0.05, n=57
ksr-2	0.14±0.03, n=478	0.44±0.08, n=174	5.80±0.35, n=90	2.66±0.15, n=348	NA
kin-18;ksr-2	0.05±0.01, n=482	1.30±0.24, n=161	7.25±0.34, n=183	2.81±0.12, n=602	NA

Number of foci are presented as Average±SE. Half nuclei of 5 gonads were counted for wild type and *ksr-2*. *kin-18* and *kin-18;ksr-2* mutants do not have a well formed rachis, three layers of nuclei of the nuclei from 7 gonads were counted for each type. NA, no nuclei of this stage is observed.

Table S5. The p value of RAD-51 foci number in different meiotic stages

Type	Wild Type	*kin-18*	*ksr-2*	Stage
kin-18	p<0.001			Early Pachytene
ksr-2	p<0.001	p>0.05		
kin-18;ksr-2	p<0.001	p>0.05	p<0.05	
Type	Wild Type	*kin-18*	*ksr-2*	Stage
kin-18	p<0.001			Middle Pachytene
ksr-2	p<0.001	p<0.001		
kin-18;ksr-2	p<0.001	p<0.001	p>0.05	

Two tailed Mann-Whitney Test were performed with 95% C.I.

Table S6. The p value of RAD-51 foci between stages with highest RAD-51 level

	kin-18	*ksr-2*	*kin-18; ksr-2*
Wild Type	$p<0.001$	$p<0.001$	$p<0.001$

RAD-51 foci of nuclei in middle pachytene from wild type were analyzed against that of nuclei in early pachytene in *kin-18*, *ksr-2*, and *kin-18;ksr-2* mutants. Two tailed Mann-Whitney Test were preformed with 95% C.I.

Table S7. The average number of RAD-51 foci by stage and by zone

		Wild Type					*kin-18*					*ksr-2*				*kin-18; ksr-2*			
Zone		PMT	TZ	EP	MP/LP	Dip/Dia	PMT	TZ	EP	MP/LP	Dip/Dia	PMT	TZ	EP	MP/LP	PMT	TZ	EP	MP/LP
1	Av.	0.26	NA	NA	NA	NA	0.15	0.15	0.43	NA	NA	0.1	NA	NA	NA	0.06	1.31	NA	NA
	%	100	0	0	0	0	84	14	2	0	0	100	0	0	0	97	3	0	0
	n	163	0	0	0	0	315	54	7	0	0	160	0	0	0	445	16	0	0
2	Av.	0.13	0.19	NA	NA	NA	0.22	0.38	7.07	7.43	NA	0.19	NA	NA	NA	0.05	1.04	6.29	5.72
	%	81	19	0	0	0	4	42	39	15	0	100	0	0	0	12.3	45.3	36.3	6
	n	134	31	0	0	0	9	98	92	35	0	235	0	0	0	37	136	109	18
3	Av.	0	0.26	1.42	8.33	NA	NA	NA	7.89	5.35	NA	0.08	0.35	NA	NA	NA	5.11	8.26	4.29
	%	2	65.5	31	1.5	0	0	0	24	76	0	46	54	0	0	0	4	26	70
	n	4	128	60	3	0	0	0	44	142	0	83	99	0	0	0	9	62	166
4	Av.	NA	NA	3.53	5.82	NA	NA	NA	NA	1.97	0	NA	0.46	5.9	7	NA	NA	10.4	3.16
	%	0	0	34	66	0	0	0	0	85	15	0	49.5	42.5	8	0	0	6	94
	n	0	0	47	90	0	0	0	0	86	15	0	57	49	9	0	0	12	174
5	Av.	NA	NA	NA	4.75	NA	NA	NA	NA	0.54	0	NA	0.89	6.21	5	NA	NA	NA	1.48
	%	0	0	0	100	0	0	0	0	87	13	0	18	29	53	0	0	0	100
	n	0	0	0	115	0	0	0	0	74	11	0	18	29	52	0	0	0	112
6	Av.	NA	NA	NA	1.81	NA	NA	NA	NA	0.25	0.21	NA	NA	4.42	2.86	NA	NA	NA	1.41
	%	0	0	0	100	0	0	0	0	76	24	0	0	14	86	0	0	0	100
	n	0	0	0	91	0	0	0	0	44	14	0	0	12	73	0	0	0	39
7	Av.	NA	NA	NA	0.39	0	NA	NA	NA	0.3	0.13	NA	NA	NA	3.78	NA	NA	NA	1.04
	%	0	0	0	56	44	0	0	0	85	15	0	0	0	100	0	0	0	100
	n	0	0	0	28	22	0	0	0	46	8	0	0	0	63	0	0	0	26
8	Av.	NA	NA	NA	0	0.33	NA	NA	NA	0.22	0	NA	NA	NA	1.31	NA	NA	NA	1.29
	%	0	0	0	17	83	0	0	0	72	28	0	0	0	100	0	0	0	100
	n	0	0	0	3	15	0	0	0	23	9	0	0	0	59	0	0	0	42
> 9	Av.	NA	NA	NA	NA	0	NA	NA	NA	NA	NA	NA	NA	NA	0.86	NA	NA	NA	0.7
	%	0	0	0	0	100	0	0	0	0	0	0	0	0	100	0	0	0	100
	n	0	0	0	0	19	0	0	0	0	0	0	0	0	92	0	0	0	25
Total	Av.	0.20	0.25	2.35	3.85	0.08	0.15	0.30	6.99	2.79	0.07	0.14	0.44	5.80	2.66	0.05	1.30	7.25	2.81
	n	301	159	107	330	56	324	152	143	450	57	478	174	90	348	482	161	183	602

RAD-51 foci by zone and stage. Av.= Average, % =percent of nuclei in each stage in the zone and mutant indicated. n number of nuclei counted for a particular zone and stage indicated.

Table S8. The p value of COSA-1 foci number in different meiotic stages

Type	Wild Type	*kin-18*	*ksr-2*	Stage
kin-18	p<0.001			Early Pachytene
ksr-2	p>0.05	p<0.001		
kin-18;ksr-2	p<0.001	p>0.05	p<0.001	
Type	Wild Type	*kin-18*	*ksr-2*	Stage
kin-18	p<0.001			Middle/Late Pachytene
ksr-2	p<0.01	p<0.001		
kin-18;ksr-2	p<0.01	p<0.001	p<0.001	

Two tailed Mann-Whitney Test were performed with 95% C.I.

File S1. Supporting Figure Legends

Figure S1. Predicted protein domain of KIN-18.

A) Effect of *ok395* mutation on the *kin-18* mRNA. Gene structure of the mRNA in wild type and kin-18 mutants, exons indicated in green. Exons missing in the deletion mutant are in purple. Note that the mRNA of the mutant is missing larger portion of the CDS than predicted by the genomic sequence due to splice site selection at the 5' of exon 8. B) Effect of *ok395* mutation on the KIN-18 protein. KIN-18a isoform codes for a protein with 982 amino acids (aa) with a predicted kinase domain and predicted target-binding domain. The *ok395* allele is predicted to result in an in-frame deletion removing most of the predicted kinase domain and the target binding domain. The *ok395* allele is predicted to result in out of frame deletion removing most of the coding region of KIN-18 b form.

Figure S2. Number of PH3 positive but not percentage of PH3 positive mitotic nuclei is reduced in kin-18 mutants.

Images of representative mitotic tip of gonads from A) wild type B) *kin-18* stained by DAPI (blue) and PH3 (green). Images are projection of panels from half gonad in wild type and one layer of nuclei in the germline in *kin-18*. Scale bar 10um. C) Number of PH3 positive nuclei in wild type and *kin-18*. ** $p<0.01$ (Mann-Whitney two-tailed test, 95% C.I.). D) Percentage of PH3 positive nuclei in mitotic tip in wild type and *kin-18*. Average numbers of mitotic tip nuclei are obtained from separate experiments. Mitotic tip and transition zone boundary is defined as in materials and methods. E) PH3 localization in oocytes of the indicated genotypes, gonads stained by DAPI (blue) and PH3 antibodies (green). Scale bar 2μm,. F) Quantitative analysis of the localization pattern of

PH3 in oocytes of the indicated genotypes.

Figure S3. SYP-1 and HIM-3 morphology in wild type and *kin-18* worms

Images of nuclei at different stages of A-F) wild type and G-L) *kin-18* mutants. MT-Mitotic Tip, TZ-Transition Zone, EP-Early Pachytene, MP-Middle Pachytene, DP-Diplotene, DK-Diakinesis. M) Images of proximal end of *kin-18* have nuclei with mixed stages. Merge: Merge of DAPI, SYP-1, HIM-3 channels. Blue: DAPI, Red: SYP-1, Green: HIM-3. Scale bar 2μm.

Figure S4. Membrane stain of wild type and *kin-18* mutants

Images of representative nuclei in the proximal gonadal region A) wild type B) *kin-18* C) quantitative analysis of cell width (see material and Methods). Merge: DAPI and Agglutinin. Blue: DAPI, Green: Agglutinin. Scale bar 10μm.

Figure S5. GLD-1 localization in Middle pachytene

Images of representative germlines in A) wild type B and C) *kin-18*. Insets are zoom in images for the regions indicating. Note the mixed GLD-1 positive and negative nuclei in the proximal gonad in *kin-18* mutants. Merge of Blue: DAPI, Green: GLD-1. Scale bar 10μm in whole gonad image, 2μm in zoom in images.

Figure S6. RAD-51 Loading in Middle pachytene in different mutants

Images of representative nuclei in middle pachytene in A) wild type B) *kin-18* C) *ksr-2* D) *kin-18;ksr-2*. Merge: Merge of DAPI, SYP-1, RAD-51 channels. Blue: DAPI, Red: SYP-1. Scale bar 2μm.

Figure S7. RAD-51 Foci distribution in different worms by microscopic zones.

Quantification of mean RAD-51 foci per nucleus in A) wild type B) *kin-18* C) *ksr-2* D) *kin-18;ksr-2* in 42 μm² microscopic zones with schematic representation of the corresponding meiotic stages. MT-Mitotic Tip; TZ-Transition Zone; EP-Early Pachytene; M/LP-Middle and Late Pachytene. DP/DK-Diplotene and Diakinesis. Number of nuclei counted for wild type from z1 to z 11 are 163, 165, 195, 137, 115, 91, 50, 18, 12, 5, 2 (from half nuclei from 5 gonads were counted); for *kin-18,* from z1 to z8 are 376, 234, 186, 101, 82, 58, 54, 32 (three layers of nuclei were counted from 7 gonads); for *ksr-2* from z1 to z13 are 160, 235, 182, 115, 99, 85, 63, 59, 43, 26, 19, 0, 6 (z12 is devoid of nuclei, half nuclei from 5 gonads were counted), for *kin-18;ksr-2*, from z1 to z10 are 461, 300, 237, 186, 112, 39, 26, 42, 20, 5 (three layers of nuclei were counted for 7 gonads).

Figure S8 Nuclei with 6 COSA-1 foci distribution in different worms by microscopic zones.

The schematic representation of the zones corresponding to the meiotic stages and the percentage of nuclei with different number of COSA-1 foci in A) wild type B) *kin-18* gonads with diplotene. MT-Mitotic Tip; TZ-Transition Zone; EP-Early Pachytene; M/LP-Middle and Late Pachytene. DP/DK-Diplotene and Diakinesis. Number of nuclei scored from z1-z8 and z9-13 for wild type are 152, 172, 139, 167, 134, 85, 50, 29, 26 (half nuclei scored from 5 gonads); for *kin-18* from z1-z9 are 351, 270, 196, 136, 119, 81, 55, 43, 23 (three layer of nuclei from 7 gonads scored);
); for *ksr-2* z1-z8 are 211, 180, 175, 144, 129, 103, 67, 48, and z9-z15 are 65 (half nuclei scored from 5 gonads); for *kin-18;ksr-2* z1-z8 and z9-z11 are 311, 235, 182, 133, 79, 26, 19, 6 and 21 (three layers of nuclei from 7 gonads).

Figure S9 Colocalization of RAD-51 and COSA-1

Images of representative germlines in A) wild type B) *kin-18* C) *ksr-2* and D) *kin-18;ksr-2* double mutants. Left: Merge of Blue: DAPI, Green: COSA-1 and Red:RAD-51. Right Merge of Green: COSA-1 and Red:RAD-51. Scale bar 10μm.

Figure S10 DAPI staining of two day old adults

DAPI stained whole worm preparation for: one day old adults of A, A' and A'') wild type B, B' and B'') *kin-18* mutants, and two day old adults of C , C' and C'') wild type D, D' and D'') *kin-18* mutants Scale bar 10μm. Each panel shows a projection of a three dimensional stack of half the gonad. A-D) zoom out A'-D'') zoom in image of representative proximal gonad nuclei that are boxed in A-D.